THE JOURNAL OF BIOLOGICAL CHEMISTRY VOL. 291, NO. 3, pp. 1411–1426, January 15, 2016

Unexpected Allosteric Network Contributes to LRH-1 Co-regulator Selectivity*

Received for publication, May 5, 2015, and in revised form, October 28, 2015 Published, JBC Papers in Press, November 9, 2015, DOI 10.1074/jbc.M115.662874

Paul M. Musille[‡1], Bradley R. Kossmann[§1], Jeffrey A. Kohn[‡1], Ivaylo Ivanov[§], and Eric A. Ortlund[‡2]

From the [‡]Department of Biochemistry, Emory University School of Medicine, Atlanta, Georgia 30322 and the [§]Department of Chemistry, Center for Diagnostics and Therapeutics, Georgia State University, Atlanta, Georgia 30302

Phospholipids (PLs) are unusual signaling hormones sensed by the nuclear receptor liver receptor homolog-1 (LRH-1), which has evolved a novel allosteric pathway to support appropriate interaction with co-regulators depending on ligand status. LRH-1 plays an important role in controlling lipid and cholesterol homeostasis and is a potential target for the treatment of metabolic and neoplastic diseases. Although the prospect of modulating LRH-1 via small molecules is exciting, the molecular mechanism linking PL structure to transcriptional co-regulator preference is unknown. Previous studies showed that binding to an activating PL ligand, such as dilauroylphosphatidylcholine, favors LRH-1's interaction with transcriptional co-activators to up-regulate gene expression. Both crystallographic and solution-based structural studies showed that dilauroylphosphatidylcholine binding drives unanticipated structural fluctuations outside of the canonical activation surface in an alternate activation function (AF) region, encompassing the β-sheet-H6 region of the protein. However, the mechanism by which dynamics in the alternate AF influences co-regulator selectivity remains elusive. Here, we pair x-ray crystallography with molecular modeling to identify an unexpected allosteric network that traverses the protein ligand binding pocket and links these two elements to dictate selectivity. We show that communication between the alternate AF region and classical AF2 is correlated with the strength of the co-regulator interaction. This work offers the first glimpse into the conformational dynamics that drive this unusual PL-mediated nuclear hormone receptor activation.

Phospholipids (PLs)[3] are best known for their structural role in membranes and as synthesis material for potent signaling molecules, such as diacylglycerol, leukotrienes, and inositol phosphates. Recent evidence, however, suggests intact PLs are able to directly modulate the activity of transcription factors involved in lipid homeostasis, such as sterol regulatory element-binding protein 1 (SREBP-1), and some members of the nuclear receptor (NR) family of ligand-regulated transcription factors, including peroxisome proliferator-activated receptor α (PPARα; NR1C1), steroidogenic factor 1 (NR5A1), and human liver receptor homolog-1 (LRH-1; NR5A2) (1–4). LRH-1 regulates the expression of genes central to embryonic development, cell cycle progression, steroid synthesis, lipid and glucose homeostasis, and local immune function (5–12). Thus, LRH-1 is an enticing pharmaceutical target for the treatment of metabolic and neoplastic diseases (6).

Although the endogenous ligand for hLRH-1 is currently unknown, oral treatment with the exogenous PL agonist dilauroylphosphatidylcholine (PC 12:0–12:0; DLPC) lowers serum lipid levels, reduces liver fat accumulation, and improves glucose tolerance in an LRH-1-dependent manner in a diabetic mouse model (13). Activation of LRH-1 by DLPC drives increased glucose uptake by muscle and increases the rate of both glycolysis and glycogen synthesis with a concomitant reduction in fatty acid metabolism (14). These observations suggest LRH-1 agonists may resolve glucose homeostasis-related diseases. New evidence suggests that LRH-1 may also be targeted to relieve chronic endoplasmic reticulum stress. Activation of LRH-1 by synthetic DLPC or the small molecule RJW100 induces *Plk3*, which is required for the activation of ATF2 and the induction of its target genes, which play a key role in resolving ER stress (15). Given its potential therapeutic value, LRH-1 has been the subject of multiple attempts to identify small molecule modulators (16–19). These attempts have been met with mixed success due in part to our limited understanding of LRH-1's mechanism of activation.

We have shown that DLPC is able to bind directly to the LRH-1 ligand binding domain (LBD) and activate the receptor by affecting receptor dynamics in an alternate activation function (AF) region, encompassing the β-sheet-H6 region of the protein, to alter co-regulator binding preference (20). Importantly, it seems that DLPC may promote activation by relieving LRH-1 from repression by the non-canonical co-repressor NR SHP, which mimics a co-activator using the canonical Leu-Xaa-

* This work was supported by National Institutes of Health Grant RO1DK095750 from NIDDK (to E. A. O.), Grant R01GM110387 from NIGMS (to I. I.), and Emory-NIEHS Graduate and Postdoctoral Training in Toxicology Grant T32ES012870 (to P. M. M.), American Heart Association Predoctoral Grant 12PRE12060583, National Science Foundation CAREER Award MCB-1149521, and a Molecular Basis Diseases fellowship (to B. R. K.). The authors declare that they have no conflicts of interest with the contents of this article. The content is solely the responsibility of the authors and does not necessarily represent the official views of the National Institutes of Health.

The atomic coordinates and structure factors (codes 4PLD and 4PLE) have been deposited in the Protein Data Bank (http://wwpdb.org/).

[1] These authors contributed equally to this work.

[2] To whom correspondence should be addressed. Tel.: 404-727-5014; Fax: 404-727-2738; E-mail: eortlun@emory.edu.

[3] The abbreviations used are: PL, phospholipid; LRH-1, liver receptor homolog-1; DLPC, dilauroylphosphatidylcholine; AF, activation function; PPAR, peroxisome proliferator-activated receptor; PDB, Protein Data Bank; DLPE, dilauroylphosphatidylethanolamine; DCIA, 7-diethylamino-3-((4′-(iodoacetyl)amino)phenyl)-4-methylcoumarin; PC, phosphatidylcholine; NR, nuclear receptor; PS, phosphatidylserine; SHP, the small heterodimer partner; PG, phosphatidylglycerol; MD, molecular dynamics; r.m.s.d., root mean square deviation; HDX, hydrogen-deuterium exchange.

Xaa-Leu-Leu (where Xaa is any amino acid) nuclear co-activator interaction motif (21, 22). In the absence of ligand, the alternate AF is highly dynamic and mutations that restrict motion in this region ablate transactivation (20). SHP is a robust co-repressor of LRH-1-mediated transactivation in the liver and can recognize both apo-LRH-1 and LRH-1 when bound to a non-ideal ligand such as bacterial PLs *in vitro* (21, 23, 24). It is unclear how LRH-1 discriminates between SHP and co-activators such as TIF2 that bind using a similar L*XX*LL motif to recognize the active NR orientation. Furthermore, how does human LRH-1 recognize co-activators in the absence of ligand? How do PLs varying only in their acyl tail composition show differing abilities to drive transactivation? Which ligand/co-regulator states are appropriate for *in silico* ligand design?

This incomplete understanding of what dictates LRH-1's PL and co-regulator selectivity limits our ability to guide the design of robust small molecule modulators for this intriguing pharmacological target. To address these questions, we have generated a novel crystal structure of the LRH-1·TIF2 complex in an apo-state, as well as a higher resolution structure of LRH-1 bound to *Escherichia coli* PLs. These crystal structures, in combination with novel lipid binding assays, molecular dynamics simulations, and principal component analysis (PCA) have allowed us to identify an unexpected allosteric network that may contribute to PL-mediated NR signaling and co-regulator selectivity.

Experimental Procedures

Reagents—Chemicals were purchased from Sigma, Fisher, or Avanti PLs. pMALCH10T and the vector for His-tagged tobacco etch virus were a gift from John Tesmer (University of Texas at Austin). pLIC_MBP and pLIC_HIS were gifts from John Sondek (University of North Carolina at Chapel Hill). Peptides were synthesized by RS Synthesis (Louisville, KY). DNA oligonucleotide primers were synthesized by IDT (Coralville, IA).

Protein Expression and Purification—The human LRH-1 LBD (residues 291–541) was purified as described previously (25). Purified protein was dialyzed against 60 mM NaCl, 100 mM ammonium acetate (pH 7.4), 1 mM DTT, 1 mM EDTA, and 2 mM CHAPS and concentrated using centrifugal filters with a 10-kDa cutoff to 5–7 mg ml^{-1}. For apo-LRH-1 crystallization, purified LRH-1 LBD was incubated with 1,2-ditetracosanoyl-*sn*-glycero-3-phosphocholine (PC 24:0–24:0) (Avanti Polar Lipids) and GSK8470, a weak and labile agonist, at a final PC24/ligand/protein ratio of 20:3:1 (17). The receptor was purified away from unbound PC 24:0–24:0 and the weakly bound agonist by size exclusion chromatography, dialyzed against 60 mM NaCl, 100 mM ammonium acetate (pH 7.4), 1 mM DTT, 1 mM EDTA, and 2 mM CHAPS and concentrated to 5–7 mg ml^{-1}.

Structure Determination—Both the apo-LRH-1 LBD·TIF2 complex and the LRH-1 LBD·*E. coli* PL·TIF2 complex crystals were generated by hanging-drop vapor diffusion at 20 °C from solutions containing 1 μl of protein at 6.5 mg ml^{-1} in complex with a peptide-derived human TIF2 NR box 3 ($+H_3N$-KENALLRYLLDKDD-CO_2-) at a 1:4 molar ratio and 1 μl of the following crystal mixture: 0.7–1 M di-sodium malonate, 0.1 M HEPES (pH 7.4), 0.5% Jeffamine ED-2001. Crystals were cryoprotected in crystallant containing 20% (v/v) glycerol and flash-frozen in liquid N_2. Data for the apo-LRH-1 LBD·TIF2 NRBox3 complex were collected to 1.75 Å resolution at 100 K using a wavelength of 0.9999 at 22-bending magnet at the Southeast Regional Collaborative Access Team (SER-CAT) at the Advanced Photon Source and were processed and scaled with HKL2000 (26). Data for the LRH-1 LBD·*E. coli* PL·TIF2 complex were collected to 1.75 Å resolution at 100 K using a wavelength of 0.9999 Å at 22-ID at the Southeast Regional Collaborative Access Team (SER-CAT) at the Advanced Photon Source and were processed and scaled with HKL2000 (26). Initial phases for both structures were determined using LRH-1 PDB code 1YOK as a molecular replacement search model. The structures were refined using the PHENIX suite of programs, and model building was carried out in COOT (27, 28). The final model for the LRH-1·TIF2 complex contains LRH-1 residues 300–538 and TIF2 residues 742–752; it shows good geometry, with 98.4 and 1.6% of the residues in the favored and allowed regions of the Ramachandran plot, respectively. The final model for the LRH-1·*E. coli* PL·TIF2 NRbox3 complex contains LRH-1 residues 298–538 and TIF2 residues 743–750; it shows good geometry, with 98.7 and 1.3% of the residues in the favored and allowed regions of the Ramachandran plot, respectively. Data collection and refinement statistics are listed in Table 1. Coordinates and structure factors have been deposited with the Protein Data Bank under accession codes 4PLD and 4PLE.

TABLE 1
Data collection and refinement statistics (molecular replacement)

	LRH-1·TIF2 NRbox3	LRH-1·*E. coli* PL·TIF2 NRbox3
Data collection		
Space group	$P2_12_12_1$	$P2_1$
Cell dimensions		
a, *b*, *c* (Å)	45.8, 65.7, 83.5	65.9, 76.9, 100.8
α, β, γ (°)	90.0, 90.0, 90.0	90.0, 95.5, 90.0
Resolution (Å)	1.75 (1.81-1.75)[a]	1.75 (1.81-1.75)[a]
R_{merge}	6.6 (30.6)	6.6 (30.9)
$I/\sigma I$	18.99 (2.8)	12.8 (3.2)
Completeness (%)	99.4 (96.22)	92.6 (63.8)
Redundancy	3.9 (3.3)	3.6 (3.2)
Refinement		
Resolution (Å)	1.75	1.75
No. of reflections	25,933	6751
R_{work}/R_{free}	18.7/22.4	21.4/23.6
No. of atoms		
Protein	2026	9019
Ligand/ion	42	493
Water	137	381
B-factors		
Protein	23.9	31.6
Ligand/ion	29.2	35.2
Water	29.4	35.2
r.m.s.d.		
Bond lengths (Å)	0.008	0.004
Bond angles (°)	1.41	0.71
PDB	4PLD	4PLE

[a] Data were collected from a single crystal. Values in parentheses are for highest resolution shell.

Local Conformational Analysis—ProSMART is an alignment tool that provides a conformation-independent structural comparison of two proteins based upon the alignment of corresponding overlapping fragments of the protein chains (29). We performed ProSMART analyses among five LRH-1 structures with different bound ligands and co-regulator peptides, repre-

senting different activation states as follows: apo-SHP (fully repressed; PDB code 4DOR); apo-TIF2, *E. coli* PL·SHP (PDB code 1YUC); *E. coli* PL−TIF2, and DLPC·TIF2 (fully activated; PDB code 4DOS). This allowed for a detailed analysis of the local structural dissimilarities between two proteins independently of their global conformations. The local backbone conformation of available LRH-1 crystal structures was compared to generate the Procrustes score, which is the r.m.s.d. of the central residue of two corresponding structural fragments of length *n*, where *n* is an odd number of amino acids.

Synthesis of NBD-DLPE—Dilauroylphosphatidylethanolamine (DLPE; 50 mg, 90 μmol), 4-chloro-7-nitrobenzofuran (NBD-Cl; 50 mg, 250 μmol), and triethylamine (17.5 μl) were dissolved in 5 ml of 1:1 $CHCl_3$/MeOH and stirred for 2 h at room temperature. The reaction mixture was dried, reconstituted in a minimal volume of $CHCl_3$, and purified by TLC on silica in 9:1 $CHCl_3$/MeOH (R_f = 0.36). The product was extracted with $CHCl_3$, filtered, and evaporated to yield 37 mg (50 μmol, 56% yield) of NBD-DLPE. Product identity and purity were verified by mass spectrometry, with a single peak corresponding to NBD-DLPE at *m*/*z* 741.38671.

Phospholipid Binding Assays—To characterize PL binding, we developed an equilibrium-based FRET assay using DCIA-labeled LRH-1 LBD as the donor and NBD-DLPE as the acceptor. Recombinant LRH-1 from *E. coli* was fluorescently labeled with DCIA (7-diethylamino-3-((4′-(iodoacetyl)amino)phenyl)-4-methylcoumarin; Molecular Probes, Inc., Eugene, OR), according to manufacturer instructions, and further purified by gel filtration chromatography to remove excess dye. All experiments were performed in assay buffer containing 150 mM NaCl, 10 mM Tris-HCl (pH 7.4), 5% glycerol, and 0.1% *N*-octyl β-D-glucopyranoside. All PL stocks were prepared as small unilamellar vesicles via sonication from evaporated chloroform stocks reconstituted in assay buffer. The binding affinity of NBD-DLPE to LRH-1 was measured using a constant concentration of 150 nM unlabeled or DCIA-LRH-1 and 0–100 μM NBD-DLPE. Competition assays were performed with constant concentrations of 150 nM DCIA-LRH-1 and 5 μM NBD-DLPE, with 0–100 μM competing PL. Fluorescence intensity was measured on a Synergy 4 plate reader (Biotek; Winooski, VT) equipped with 380/20 nm excitation and 460/40 nm emission filters. All assays were performed in triplicate on black 384-well plates in a total volume of 50 μl. Data for unlabeled LRH-1 were subtracted from corresponding DCIA-LRH-1 data to remove background fluorescence, and all background-corrected data were expressed as percent fluorescence intensity of fully unbound DCIA-LRH-1 (*i.e.* 0 M NBD-DLPE). Data were processed with GraphPad Prism 5 (GraphPad Software, Inc.).

Reporter Gene Assays—Transactivation of wild type and mutant LRH-1 was measured via luciferase-based reporter gene assay. HEK 293T cells were seeded into 24-well plates and incubated at 37 °C in complete media (DMEM supplemented with 10% charcoal/dextran-stripped FBS and 1% penicillin/streptomycin) until ~90% confluent. Each well was then transiently transfected in OptiMEM using Lipofectamine 3000 with plasmids encoding firefly luciferase under control of the *shp* promoter (SHP-luc; 500 ng/well), *Renilla* luciferase under constitutive activation via the CMV reporter (pRLCMV; 10 ng/well), and wild type or mutant LRH-1 in the pCI mammalian expression vector (100 ng/well). Transfection was ended after 4 h of incubation at 37 °C via the replacement of transfection mixture with complete media, and cells were incubated overnight. Luciferase activity was measured using the Dual-Glo luciferase assay system (Promega; Madison, WI). Statistical analyses were performed in GraphPad Prism 5 (GraphPad Software, Inc., La Jolla, CA), via one-factor analysis of variance followed by Dunnett's multiple comparison test using wild type LRH-1 as a control. Data are the results of five independent experiments. All mutations were introduced into the wild type LRH-1/pCI construct using the QuikChange II Lightning multisite-directed mutagenesis kit (Agilent Technologies, Inc., Santa Clara, CA).

Model Construction for Molecular Dynamics—Five models were constructed to examine the structural and allosteric impacts of ligand/co-regulator agreement as follows: 1) apo-LRH-1·TIF2 NRBox3; 2) LRH-1·DLPC·TIF2 NRBox3, 3) LRH-1·*E. coli* PLs·TIF2 NRBox3; 4) apo-LRH-·SHP NRBox2; 5) LRH-1·*E. coli* PLs·SHP NRBox2. Agreement is defined here by simultaneous binding of an activating lipid and co-activator or by the binding of a co-repressor in the absence of ligand. In every case, residues 297–540 from the LRH-1 LBD form the core of the complex, with additions of 2–3 residues at either terminus as necessary to maintain consistent sequences between models, using the program Xleap, part of the AmberTools11 suite (30). All five systems were solvated with TIP3P water in a rectangular box with equilibrated dimensions of 67 × 70 × 72 Å and neutralized with sodium and chloride ions to a salt concentration of 0.15 M.

Briefly, the first model containing the LRH-1 LBD, in the apo-state, bound to a TIF2 co-activator peptide was modeled directly from the novel apoLRH-1·TIF2 NRBox3 crystal structure. The second model, containing DLPC in the binding pocket, bound to a TIF2 co-activator peptide was modeled directly from PDB code 4DOS (20). The third system, comprised of the LRH-1 LBD with the *E. coli* PL in the binding pocket, bound to a TIF2 peptide was modeled from the novel LRH-1·*E. coli* PLs·TIF2 NRBox3 crystal structure. Although electron density in the crystal structure is insufficient to identify the headgroup of the bound lipid, mass spectrometry results suggest phosphatidylglycerol and phosphatidylethanolamine to be the predominant PL isoforms (20). Thus, we modeled a bacterial phosphatidylethanolamine with 16 and 18 carbons on the *sn*1 and *sn*2 position, respectively, derived from the PDB ligand EPH, which is herein referred to as *E. coli* PL. The fourth model consists of the LRH-1 LBD, in the apo-state, bound to a SHP co-repressor peptide, constructed from the LRH-1 LBD (derived from the apoLRH-1 LBD-TIF2 NRBox3 structure), with the SHP peptide (PDB code 4DOR) (20) modeled in place of TIF2 via superposition of LRH-1 LBD residues 340–382 and 533–538. The charge clamp-specific contacts between LRH-1 residues Arg-361 and Glu-534 and the SHP peptide were enforced with harmonic restraints during the equilibration phase of the molecular dynamics simulation and released before the production runs. The final model, LRH-1 containing DLPC in the binding pocket and bound to an SHP co-repressor peptide, was constructed from PDB code 4DOS

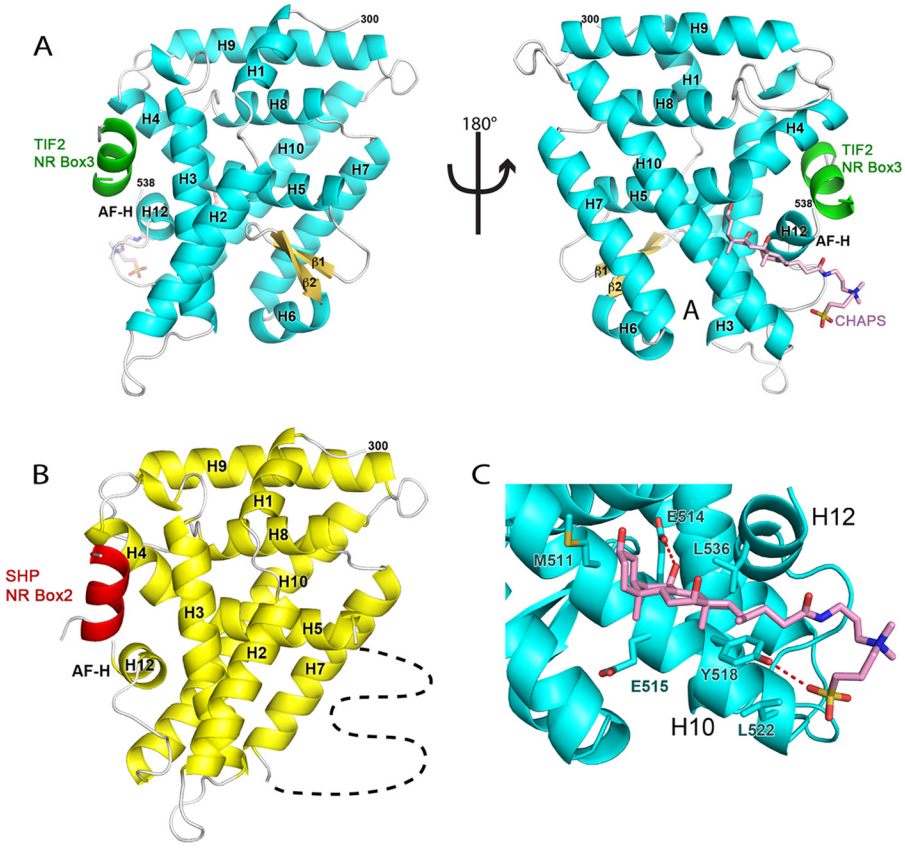

FIGURE 1. **Structure of the apo-LRH-1 LBD·TIF complex.** *A*, *ribbon diagram* of apo-LRH-LBD (α-helices, *teal*; β-strands, *yellow*) with the TIF2 NR box 3 peptide (*orange*). The surface-bound CHAPS is depicted as *sticks* (C, *pink*; O, *red*; S, *yellow*; N, *blue*). The AF-2 surface is defined by H3, H4b and H12. *B*, *ribbon diagram* of apo-LRH·SHP NRBox2 complex (PDB code 4DOR) with the unobserved alternate AF region (defined by β1–2 and H6) represented by a *dashed line*. *C*, close-up view of the bound CHAPS molecules included in the crystallization buffer.

(20) with the SHP co-repressor modeled in place of TIF2 as described in the previous model.

Molecular Dynamics—The CHARMM27 (31) force field for lipids and proteins was employed for all simulations. All systems were subjected to 10,000 steps of steepest-descent minimization, heated to 300 K under the canonical ensemble for 100 ps. Finally, positional restraints were incrementally released first on the protein side chains, followed by the backbone, under the isobaric-isothermal ensemble. Production runs were performed under constant pressure and temperature, totaling 212 ns of unrestrained molecular dynamics for each system, with 12 ns discarded as equilibration, resulting in 200 ns of production simulation time per system. All simulations were performed with NAMD 2.9 (32), employing the r-RESPA (33) multiple time step method, with bonded and short range interactions evaluated every 2 fs and long range electrostatics evaluated every 4 fs with the smooth Particle Mesh Ewald method (34). The short range non-bonded interactions were calculated using a cutoff of 10 Å with a switching function at 8.5 Å. The integration time step was 2 fs and the SHAKE algorithm was applied to fix the bonds between the hydrogens and the heavy atoms. Parameters and topology for the *E. coli* PL ligand were obtained from the general lipid parameters available in CHARMM27.

Analysis Methodology—For all analyses, 10,000 evenly spaced frames were taken from the 200-ns production runs to allow for sufficient statistical sampling. Covariance matrices were constructed using the program Carma (35) over all α-carbons to produce per-residue statistics. The Network View plugin (36) in VMD (37), along with the programs subopt, included in the Network View package, and Carma were employed to produce dynamical networks for each system, along with suboptimal path analyses. The ptraj module of AmberTools11 was used for structural averaging as well as Cartesian principal component analysis over protein backbone atoms and over the same 10,000-frame trajectories used for the covariance analyses. Principal components were projected onto the molecular dynamics trajectories, with snapshots binned according to their displacements along the components. Temporal correlations between modes are lost in this approach, but heavily sampled regions of the conformational subspace are more easily identified.

Results

Structure of the Apo-LRH-1 LBD·TIF Complex—LRH-1 is able to bind to both co-activators and co-repressor proteins in the absence of a ligand. To visualize the structural perturbations necessary to bind to co-activators in its apo-form, we crystallized apo-LRH-1 LBD bound to a fragment of the co-activator TIF2 and determined its structure to 1.75 Å (Fig. 1*A*). There is no visible electron density to support modeling a bound ligand. The opening to the ligand binding pocket is constricted by 2 Å, which reduces the volume of the ligand binding pocket from 1554 $Å^3$ in the LRH-1·TIF2·DLPC complex to roughly 940 $Å^3$ (Fig. 4, *A versus B* and *D*). This is in stark

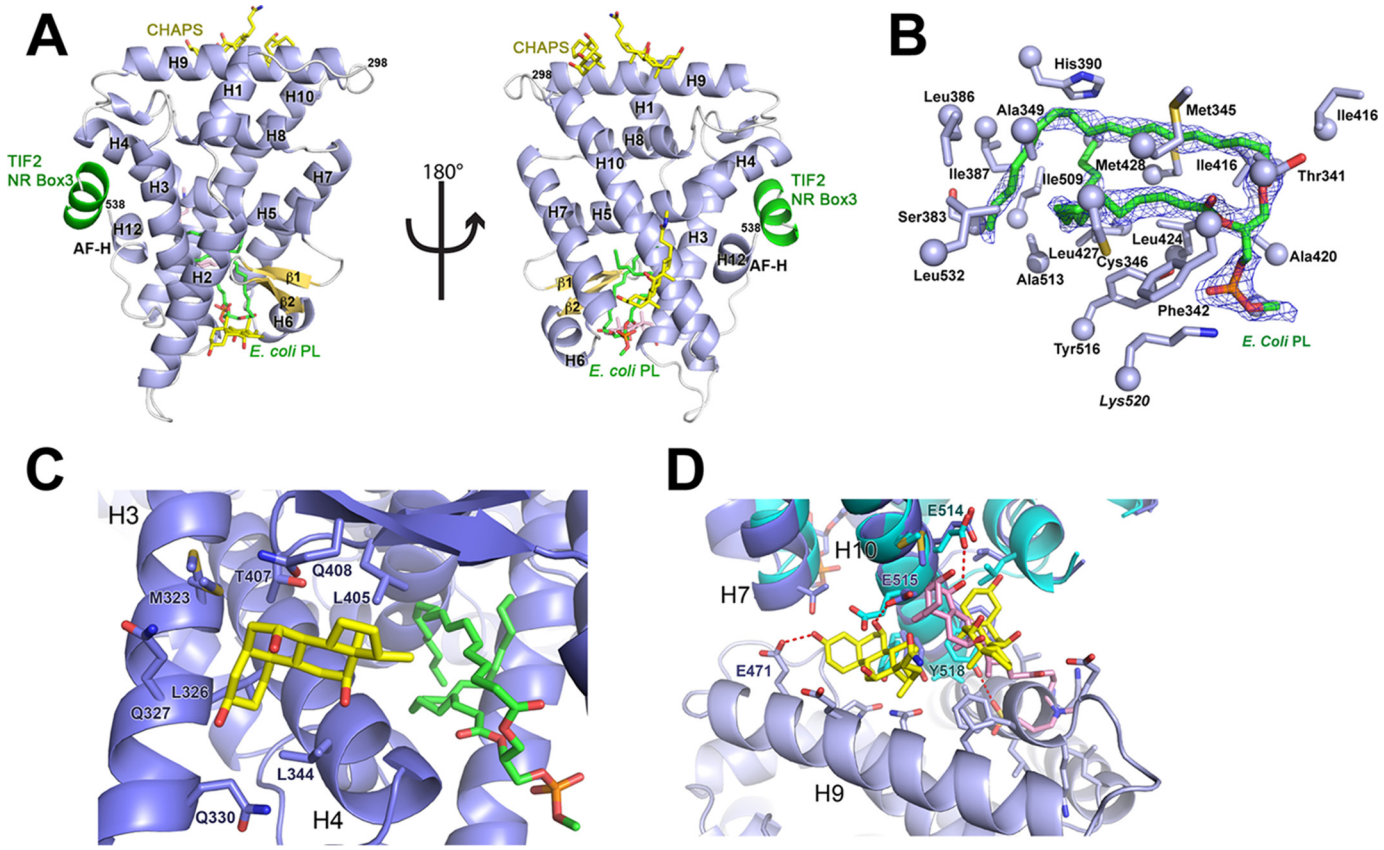

FIGURE 2. **Structure of the LRH-1 LBD·*E. coli* PL·TIF2 complex.** *A, ribbon diagram* of *E. coli* PL-bound LRH-LBD (α-helices, *teal*; β-strands, *yellow*) with the TIF2 NR box 3 peptide (*green*). The bound *E. coli* PL is depicted as sticks (C, *green*; O, *red*; P, *magenta*) The surface-bound CHAPS is depicted as *sticks* (C, *yellow*; O, *red*; S, *yellow*; N, *blue*). *B*, $2F_o - F_c$ electron density (contoured at 1 σ) for the bound *E. coli* PL observed in this structure, along with side chains lining the ligand binding pocket of hLRH-1 that contact this ligand. *C*, close-up view of the bound CHAPS molecules included in the crystallization buffer along H3 and H4 in close proximity to the bound PL. Residues within 4.2 Å are depicted as *sticks*. *D*, close-up view of the bound CHAPS along H9, which interact with a crystallographic symmetry mate and in a position overlapping the CHAPS site in the apo-LRH-1·TIF2 complex. Residues within 4.2 Å of CHAPS are depicted as *sticks*.

contrast to the apo-LRH-1 LBD-SHP NRBox2 structure reported previously, which lacks electron density for the entirety of the alternate AF (Fig. 1, *A versus* C). Unlike the ligand binding pocket of rodent LRH-1, the ligand binding pocket constriction is not stabilized by any intramolecular interactions (38). However, it is possible that the alternate AF, which comprises nearly one-third of the binding pocket, may be visible due to fortuitous interactions with a crystallographic symmetry mate. Regardless, this shows remarkable flexibility of the ligand binding pocket.

The structure contains a single CHAPS detergent molecule that docks on H10 and H12 via hydrophobic interactions and two hydrogen bonds between the CHAPS 7-OH and Glu-514, and the CHAPS phosphate and Tyr-518. CHAPS also makes extensive contact with a crystallographic symmetry mate (Fig. 1*C*). Thus, two molecules within the crystal create a cleft for CHAPS binding.

Improved Structure of the LRH-1 LBD·E. coli PL·TIF2 Complex—To generate a more accurate model for molecular dynamics studies, and as a control in our crystallization experiments, we crystallized the LRH-1 LBD·*E. coli* PL·TIF2 complex and determined its structure to 1.75 Å (Fig. 2*A*). This represents an improved resolution over the existing LRH-1 LBD·*E. coli* PL·TIF2 structures, which were both solved to 2.5 Å (39, 40). The structure is highly similar to the previous structures with an r.m.s.d. of 0.6 Å over main chain atoms and maintains *E. coli* PLs in the binding pocket (Fig. 2*B*). The lipid acyl tails show a decrease in electron density near their termini, which is similar to previous observations for the bound *E. coli* PLs and the LRH-1·DLPC complex (Fig. 2*B*) (20). This observation further supports the hypothesis that LRH-1 specifically recognizes its PL ligands near the glycerophosphate backbone, and the exact position of the acyl tails is less important than the amount of space they occupy in the deeper portion of the ligand binding pocket.

The structure contains three CHAPS detergent molecules that dock onto the surface of the protein and make interactions with crystallographic symmetry mates. One CHAPS molecule is secured in the cleft between H3 and the β-sheets via hydrophobic interactions. A second CHAPS molecule mediates contact between two copies of the LRH-1 monomer and is secured by hydrophobic interactions along H10 and a hydrogen bond with Glu-515 of one monomer, and hydrophobic interactions along H9 and a hydrogen bond with Glu-471 of the second monomer. The third CHAPS is adjacent to the second, and it also mediates contact between two LRH-1 monomers via hydrophobic interactions with H10 of the first monomer and H9 of the second, but it does not make any hydrogen bonds with either monomer. The CHAPS molecules contacting two LRH-1

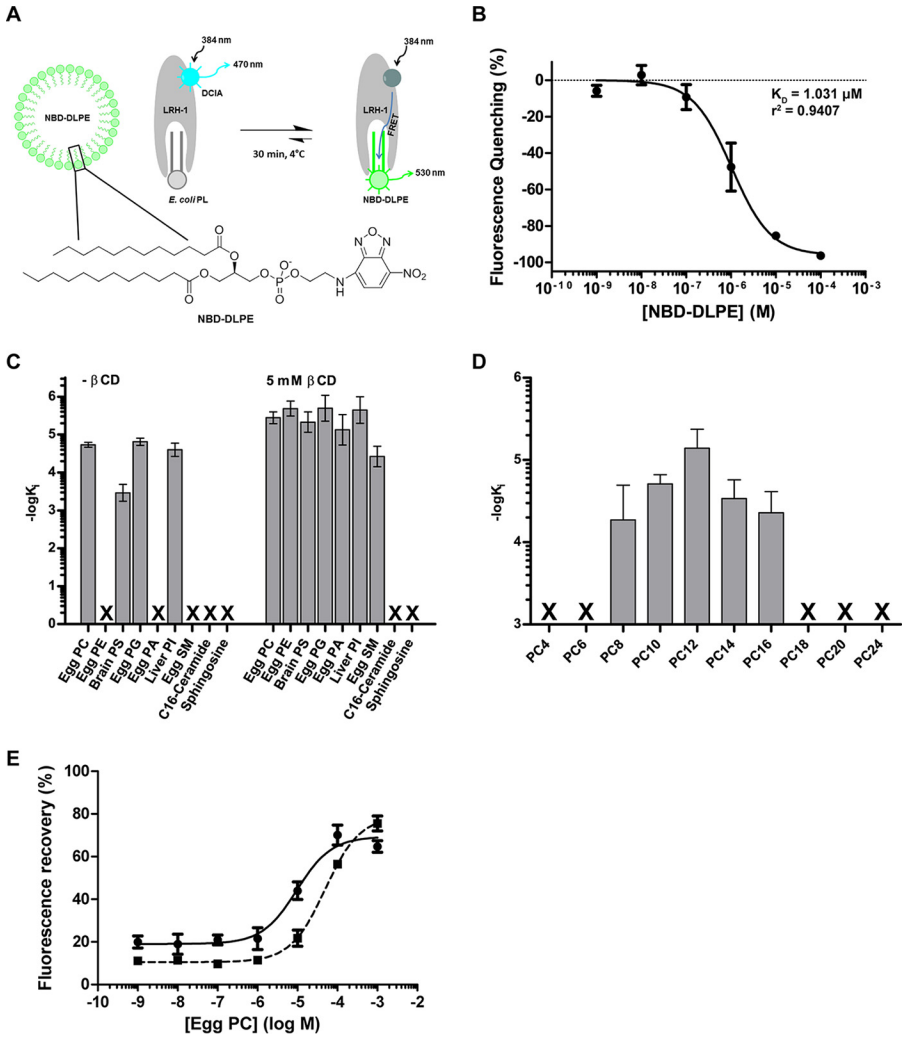

FIGURE 3. **LRH-1 *in vitro* lipid binding profile.** Binding affinities of LRH-1 to PLs of differing headgroup and tail compositions. *A*, PL binding was measured relative to probe ligand NBD-DLPE via FRET quenching of DCIA-labeled LRH-1. *B*, binding affinity of LRH-1 to NBD-DLPE probe. *C*, relative binding affinities of competing PLs of differing headgroups; 5 mM β-cyclodextrin added as indicated. *D*, relative binding affinities of competing saturated PCs of differing tail lengths. Data are reported are the means ± S.E. of three independent experiments. The presence of an × instead of a *bar* indicates that no binding was observed. *E*, example of an individual competitive binding curves for NBD-DLPE displacement. *Solid line* represents the inclusion of 5 mM β-cyclodextrin, although the *dashed line* is without 5 mM β-cyclodextrin as described under "Experimental Procedures."

monomers are unique relative to the apo-LRH-1 LBD·TIF complex, whereas CHAPS occupying the site near H10 shows a partial overlap with the well ordered CHAPS in the apo-structure (Fig. 2*D*). In contrast to the excellent electron density for the CHAPS bound in the apo-LRH-1 LBD·TIF complex, the CHAPS bound at this site in the *E. coli* lipid-bound complex shows electron density for only the sterane ring. This is likely due to greater thermal motion or reduced CHAPS occupancy at this site in the crystal. Interestingly, CHAPS is docked at regions within LRH-1 that show most exchange in HDX studies and the most conformational fluctuations in crystal structures. It is possible that these are sites for protein-protein or protein/lipid interaction in the cell.

LRH-1 can bind to several PLs (2, 25, 40, 41), yet only PCs have been shown to drive transactivation (13, 20, 40, 41). It is unclear why LRH-1 responds only to PCs in cells; this may be intrinsic to the receptor or due to uncharacterized PL transporters capable of delivering PC ligands. To elucidate the mechanisms by which PLs differentially activate LRH-1, it is critical to determine the effects of headgroup and tail variation on binding. To characterize differential PL binding, we developed a FRET-based PL binding assay monitoring the ability of NBD-labeled DLPE to bind to DCIA-labeled LRH-1 (Fig. 3*A*). This binding event quenches the DCIA fluorescence, which can be recovered upon the competitive binding of unlabeled lipids (Fig. 3, *B* and *E*).

Prior to engulfing PLs, LRH-1 must extract PL from the lipid membrane, a step typically conducted by PL transport proteins that contain amphipathic structural elements to facilitate partitioning in membranes (42–44). In the absence of lipid chaperones, we find that LRH-1 extracts and binds PC, PG, and phosphatidylinositol with micromolar affinity, but it cannot extract phosphatidylethanolamine, PS, phosphatidic acid, sphingomyelin, ceramide, or sphingosine (Fig. 3*C*). Thus, LRH-1's ability to bind PLs from vesicles is sensitive to the nature of the headgroup. However, addition of 5 mM β-cyclodextrin, a small molecule chaperone widely used for the delivery of hydrophobic small molecules, enables the binding of PC, phosphatidyletha-

nolamine, PS, PG, phosphatidic acid, with low micromolar affinity (Fig. 3*C*). LRH-1 is unable to bind sphingosine and ceramide despite the presence of β-cyclodextrin suggesting that extraction from vesicles is not a limiting factor; rather, these lipids do not fit well within the ligand binding pocket. These extracts contain a range of PL isoforms, and the PC mixture showed the highest maximum displacement of bound NBD-DLPE (Fig. 3*E* and data not shown).

We then investigated LRH-1's intrinsic selectivity for PL tail composition by testing a range of saturated PCs. Surprisingly, only PCs with mid-length chains of 8–16 carbons bind to LRH-1, with DLPC showing the strongest affinity. We observed no change in binding with the inclusion of 5 mM β-cyclodextrin (data not shown). These findings mirror previously published activation data, which demonstrate that LRH-1 is most strongly activated by the 11- and 12-carbon saturated PCs, diundecanoyl phosphatidylcholine and DLPC (13). Thus, PL selectivity is driven by the length of the fatty acid tails *in vitro* suggesting that the amount of space filled by the acyl tails is a critical determinant of binding.

Co-regulator Binding Interactions Are Altered by Ligand Status—The canonical model of NR activation revolves primarily around a mobile ligand-sensing helix (H12), termed the AF-H. When a receptor is bound to an agonist, the AF-H packs against helices 3 and 4 of the LBD forming a surface, termed activation function 2 (AF-2), which enables interaction with co-activator proteins containing an L*XX*LL motif (45). This helical peptide inserts its leucines into a groove on the AF-2 surface and is further stabilized by charge clamp interactions with Arg-361 on H3 and Glu-534 on the AF-H. An equivalent charge clamp is conserved across NRs and represents a general mechanism for activation (46). LRH-1, like some other orphan NRs, is able to form a productive AF-2 in the absence and presence of ligands in available crystal structures. This makes inferences regarding ligand potency based on backbone positioning within the AF-2 alone challenging. Nevertheless, we compared co-regulator binding at the AF-2 across all available crystal structures, and we observed that regardless of the ligand state, Arg-361 on H3 forms the expected charge clamp interaction. In contrast, we were surprised to find that Glu-534, on the AF-H, does not make the expected charge clamp interaction with co-regulator peptide under all circumstances (Fig. 4). This does not appear to be an artifact of crystal packing. Instead, the conformation of Glu-534 correlates with an agreement between the ligand and the bound co-regulator peptide. Agreement is defined here by simultaneous binding of an activating lipid and co-activator or by the binding of a co-repressor in the absence of ligand. When apo or bound to a poorly activating ligand, Glu-534 is rotated out of hydrogen bond distance with the co-activator TIF2 peptide (Fig. 4, *A–C*). In contrast, when LRH-1 is bound to a strong agonist such as DLPC, Glu-534 makes the expected hydrogen bond with a backbone amide of the TIF2 peptide (Fig. 4*D*). This charge clamp interaction is also observed in apo or *E. coli* PL-bound LRH-1 when complexed to a peptide derived from the co-repressor SHP (Fig. 4, *E* and *F*). These observations suggest that LRH-1 has an extensive allosteric network that appropriately tunes the receptors' ability to stabilize very similar L*XX*LL motifs present in co-activators and co-repressors.

Ligand and Co-regulator Drive Differential Effects on Local Residue Environment—Supposition of multiple LRH-1-ligand structures revealed only subtle differences in the co-regulator binding surface. We therefore used ProSMART to compare the local residue environment to identify how differential ligand and co-regulator peptide binding affects local structure (29). Caution of course must be taken with the interpretation of these results because the crystal structures included in this analysis are derived from multiple crystal forms.

LRH-1 shows the greatest conformational similarity between structures where both ligand and co-regulator status are in agreement within the structural complex (Fig. 5). Greater conformational dissimilarity is seen when one or both complexes are not in ligand-co-regulator agreement, indicating that such agreement is crucial in maintaining a stable complex, regardless of whether that complex is activated or repressed. In all co-regulator states, the addition of a ligand stabilizes the alternate AF region compared with apo, as demonstrated by the high structural dissimilarity seen in this region compared with the apo-TIF2 structure (Fig. 5, *E*, *F*, and *H*), and the fact that this area could not be modeled in the apo-SHP complex. As expected, the highest structural dissimilarity is seen in the AF-2 and alternate AF (β-sheets/H6), the respective interaction sites for the co-regulator peptide and PL headgroup. SHP poorly discriminates between apo and bacterial PL-bound receptor and shows high structural similarity throughout the ligand binding domain (Fig. 5*A*). In contrast, the LRH-1 TIF2 complexes show strong differences with LRH-1 SHP complexes regardless of ligand status, even in cases where the ligand is the same or nonexistent (Fig. 5, *B–E*, *G*, and *I*). Thus, unlike SHP, TIF2-bound conformations are sensitive to the nature of the bound ligand. All LRH-1·TIF2 complexes exhibit moderate or high structural dissimilarity in both the AF-H and the preceding loop and the alternate AF region (Fig. 5, *F*, *H*, and *J*). The greatest agreement among the LRH-1·TIF2 complexes is seen between the *E. coli* PL and DLPC-bound structures (Fig. 5*J*), indicating that although TIF2 is sensitive to the presence or absence of a ligand, it does not strongly discriminate between ligands so long as one is present. This is consistent with previous co-regulator recruitment studies, which show only a 3-fold difference in binding affinities between TIF2 and *E. coli* PL or DLPC-bound LRH-1 (20.1 and 6.5 μM, respectively) (20). Taken together, the ProSMART analyses suggest that ligand-co-regulator agreement promotes the stabilization of LRH-1 into either an active or repressed conformation, with detectable but subtle structural differences between these conformations. These conformational variations are also in line with the prior HDX data showing conformational variation between the same structural elements (*i.e.* the alternate AF, the AF2, and in H8 and H9) (1).

Activated LRH-1 Complex Exhibits Coordinated Motions—To analyze the dynamic coupling of structural elements in LRH-1, we computed cross-correlation (normalized covariance) matrices for the C-α atoms in each of the five systems with the program Carma (35). A covariance matrix contains a great deal of

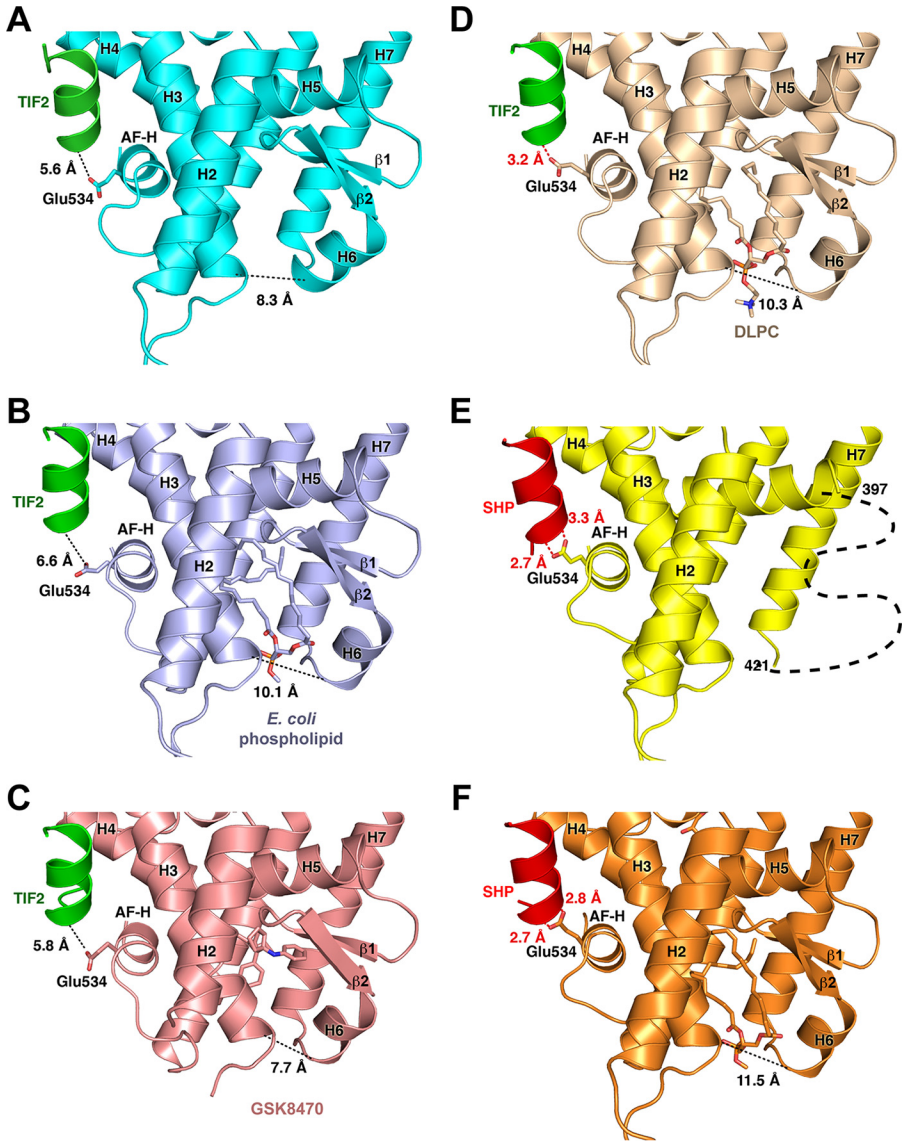

FIGURE 4. **AF-2 charge clamp engagement is dictated by ligand-co-regulator combination.** Ligand binding pocket entrance measurements and analysis of Glu-534-peptide charge clamp engagement for the apo-LRH-1·TIF2 complex (*A*), LRH-1·*E. coli* PL·TIF2 complex (*B*), LRH-1·GSK8470·TIF2 complex (PDB code 3PLZ) (*C*), LRH-1·DLPC·TIF2 complex (PDB code 4DOS) (*D*), apo-LRH-1·SHP complex (PDB code 4DOR) (*E*), and LRH-1·*E. coli* PL·SHP complex (PDB code 1YUC) (*F*) are shown.

information regarding the dynamics within a system, in this case describing the correlation of motions r_i and r_j for residues i and j, taken from their respective α carbons. Element (i, j) of the covariance matrix is calculated as $\langle(r_i - \langle r_j\rangle)(r_j - \langle r_i\rangle)\rangle$. In essence, this type of covariance matrix provides a way of visualizing whether the motions of two residues within a complex are correlated, anti-correlated, or non-correlated. A cross-correlation matrix is simply a covariance matrix that is normalized to vary between −1 (perfectly anti-correlated) and 1 (perfectly correlated) (Fig. 6).

The motions in residues within helices 4–9 of the LRH-1 LBD become correlated upon lipid binding in the presence of a co-activator (Fig. 6*C*). The correlation of these motions in the lipid and co-activator-bound systems is muted in the apo-states as well as the DLPC-bound LBD in complex with the SHP peptide (Fig. 6, *A* and *D*). This suggests that both lipid and co-regulator binding impact an allosteric network through the LRH-1 core, requiring the lipid pocket and AF-H elements to be in agreement to yield an active complex. Lipid may therefore allow correlated motions in LRH-1 to favor TIF2 binding while in the apo-state these motions are eliminated, thereby favoring SHP binding.

We have mapped cross-correlation between the lipid headgroup phosphorus atom and all protein residues, for each lipid-bound system studied, onto the LRH-1 structure (Fig. 6, *F–H*). We find that the lipid displays some positive covariance with the β-H6 region of the complex and some negative covariance with H9 and H2. The DLPC-LRH-1-SHP system shows similar behavior, but with smaller magnitudes, likely due to its disagreement status.

MD Simulations Demonstrate Communication between β-Sheet-H6 and the AF-H through Helices 3–5—We have previously discovered that LRH-1 contains an alternate activation function region that encompasses the β-sheet-H6 portion the

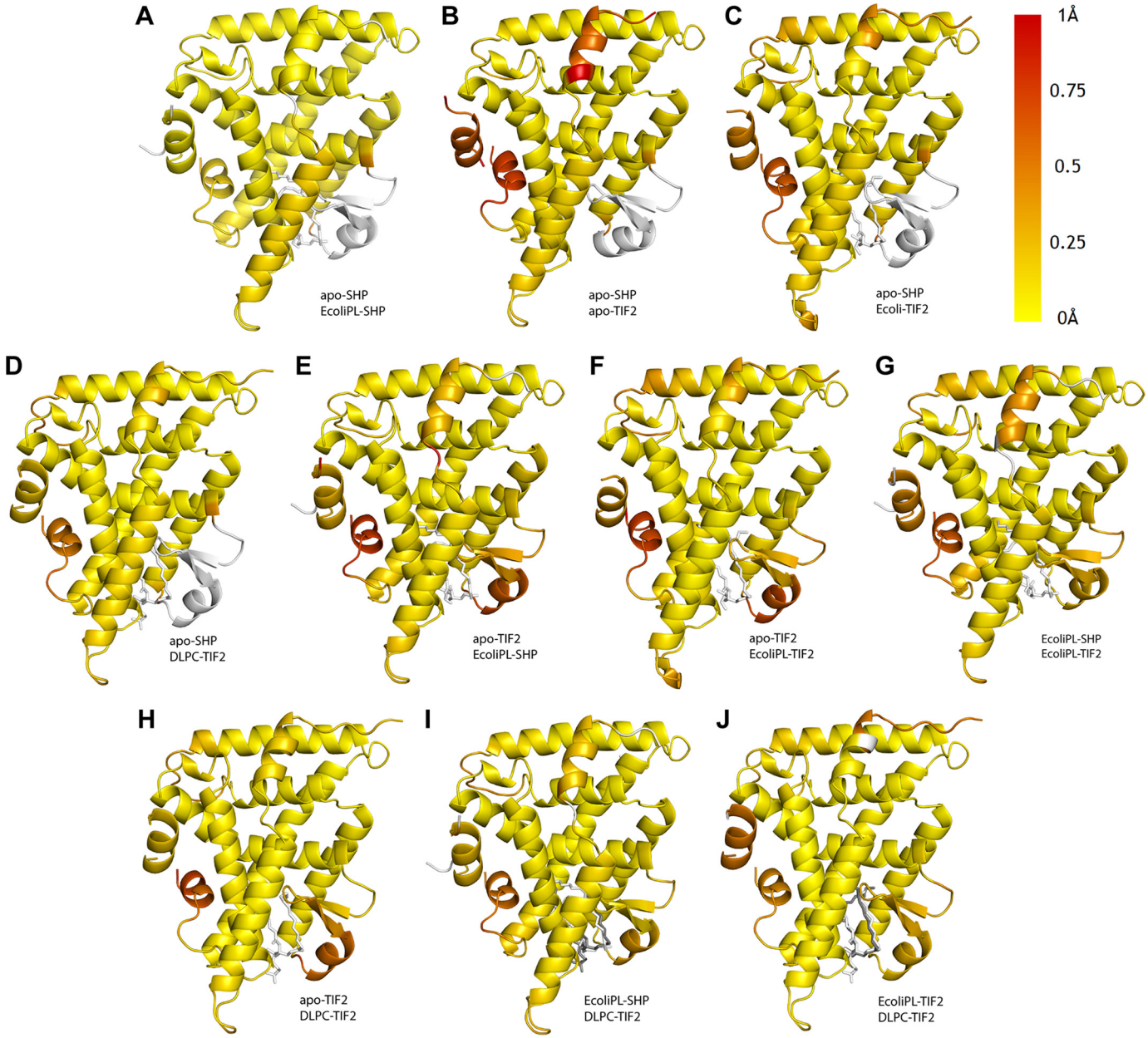

FIGURE 5. **ProSMART Procrustes central residue analysis of LRH-1 complexes.** ProSMART analysis of LRH-1 with differentially bound ligands and co-regulator peptides is shown. Models were colored by the Procrustes score of the central residue of an aligned fragment pair according to the legend at *top right*. Areas colored white were omitted from the analysis. The following pairwise comparisons were made: *A,* apo-SHP (PDB code 4DOR) *versus E. coli* PL·SHP (PDB code 1YUC); *B,* apo-SHP *versus* apo-TIF2; *C,* apo-SHP *versus E. coli* PL·TIF2; *D,* apo-SHP *versus* DLPC-TIF2 (PDB code 4DOS); *E,* apo-TIF2 *versus E. coli* PL·SHP; *F,* apo-TIF2 *versus E. coli* PL·TIF2; *G, E. coli* PL·SHP *versus E. coli* PL·TIF2; *H,* apo-TIF2 *versus* DLPC-TIF2; *I, E. coli* PL·SHP *versus* DLPC-TIF2; *J, E. coli* PL·TIF2 *versus* DLPC-TIF2.

ligand binding pocket. Our data suggested that the dynamics of this region are coupled to ligand binding and receptor activation (20). To identify the relevant communication pathways contributing to these observations, we constructed dynamical networks to identify the most prevalent communication pathways between the β-sheet-H6 region and the bound co-regulator (Fig. 6). Dynamical networks, as defined in the field of network theory, describe the communication pathways between components of a system. In a dynamical network, every component is taken to be a "node," and a communication between two nodes defines an "edge." In the methodology employed here, each protein residue's α carbon is a node, and any two nodes must be within a distance cutoff of 4.5 Å for 75% of the MD trajectory, and the strength of communication between two nodes, or the "edge weight," is determined from the covariance between the two nodes. A communication path between two distant nodes is then a chain of edges that connects them, and the optimal path transmits communication between two nodes through the fewest number of edges possible and is likely to carry more communication than any other single path. The optimal path and a relatively small set of slightly longer suboptimal paths are expected to carry the majority of communications between two edges. Monitoring the strength and number of suboptimal paths between two distant nodes can yield

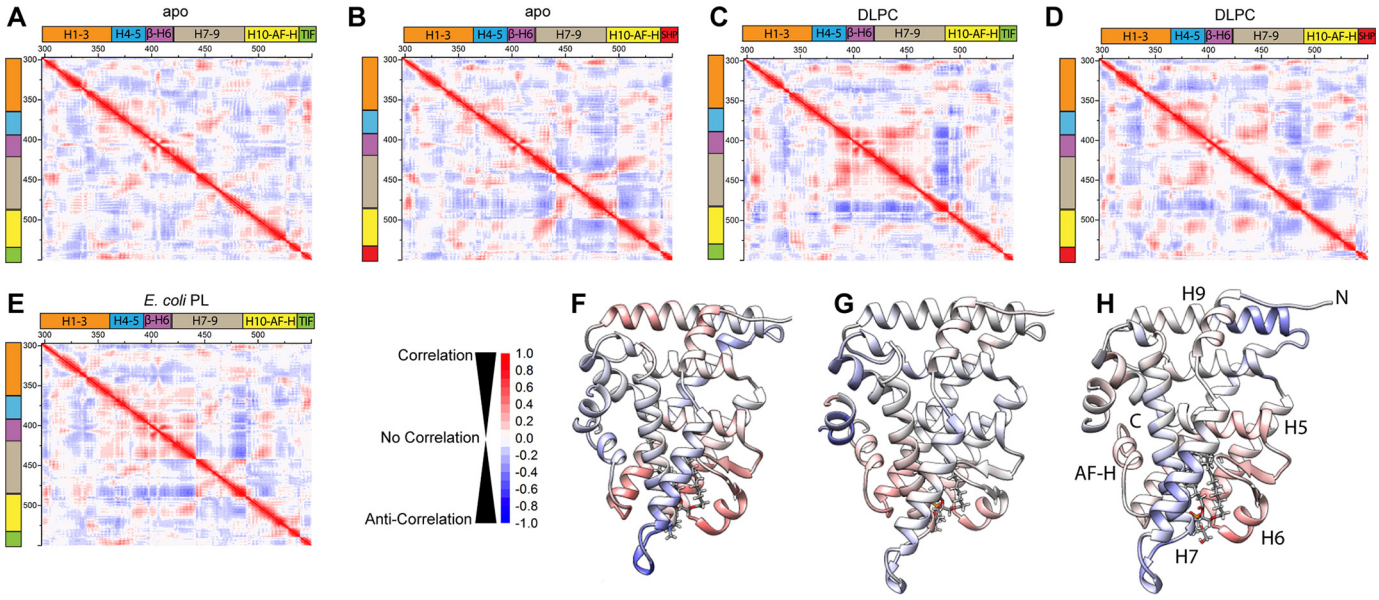

FIGURE 6. **Correlated motion in LRH-1-PL co-regulator systems.** Cross-correlation matrices showing correlated and anti-correlated motion over the 200-ns MD simulation for apo-LRH-1·TIF2 complex (*A*), apo-LRH-1·SHP complex (*B*), LRH-1·DLPC·TIF2 complex (*C*), LRH-1·DLPC·SHP complex (*D*), and LRH-1·*E. coli* PL·TIF2 complex (*E*). Cross-correlation between protein residues and the lipid headgroup phosphorus atom is mapped to the protein structure in LRH-1·DLPC·TIF2 complex (*F*), LRH-1·DLPC·SHP complex (*G*), and LRH-1·*E. coli* PL·TIF2 complex (*H*).

detailed insight into the strength of communication or, in macromolecular systems, allostery.

These pathways show much stronger communication when the lipid pocket and AF-H domain states are in agreement than otherwise (Fig. 7, *A*–*E*). The number of communication pathways increases greatly upon lipid pocket-AF-H state agreement, especially expanding outward from the β-sheet-H6 region and into the co-regulator itself. This strongly supports our previous hypothesis that the β-sheet-H6 and AF-H regions communicate to control LRH-1 activation. Furthermore, the vast majority of communication paths proceed through helices 3–5. These same helices showed the most protection from deuterium exchange in prior HDX studies suggesting that their rigidity may facilitate the flow of information through the receptor (20). Therefore, the allosteric pathway between the β-sheet-H6 region and AF-H likely traverses through helices 3–5 (Fig. 6, *B* and *D*). These helices present an optimal tether between the allosteric switches. It is interesting to note that many of the mutations that affect LRH-1 PL binding, co-regulator sensitivity, and overall activation lie directly on or immediately adjacent to this pathway (Fig. 7*F*) (20, 25, 38).

Structural and Dynamical Rationale for Lipid and Co-regulator Agreement—To identify the functionally significant collective motions of the residues forming the allosteric network within LRH-1, we employed principal component analysis (PCA) (48). In PCA, the C-α covariance matrix is diagonalized to yield eigenvectors, denoted as principal modes, and eigenvalues, representing the mean square fluctuation along each principal mode. Projections of the MD trajectory onto the principal modes are called the principal components. By reducing the dimensionality of the data, PCA recapitulates the most important dynamical features from the MD trajectories. Thus, the first few principal modes, known as the essential dynamics, are likely to describe the collective global motions of LRH-1 involved in the allosteric response to ligand and co-regulator binding.

We have identified two modes that are indicative of the lipid binding pocket's state and the bound co-regulator, named PC1 and PC2, and have projected snapshots from the molecular dynamics trajectories onto these modes in Fig. 8. To ensure comparability and uniformity of the modes studied, we optimized the total root mean square inner product across all systems' essential dynamics. The root mean square inner product method for optimizing subspace overlap does not guarantee that the same mode number will be selected from each system, as some variation in the ordering of principal modes is expected, even for highly similar systems (49). A table of the modes chosen for PC1 and PC2 and the dot products between these modes are included in Table 2.

In the projections (Fig. 8, *C*–*G*), areas of high density indicate regions of high conformational probability. Snapshots from the most densely populated regions of each system's conformational subspace were collected and averaged to obtain representative structures for comparison (Fig. 8, *A* and *B*). PC1 is characterized by an outward motion of helix 9 relative to helix 8 and the core of the LBD, with the distance from Asn-332 to Thr-422 measuring 29.1 Å in the DLPC·LRH-1·TIF2 model and 26.1 Å in the apo-LRH-1·SHP model (Fig. 8*A*). PC2 consists primarily of an opening motion near the mouth of the lipid binding pocket, with the distance from Gln-444 to Asn-487 measuring 13.9 Å in the most prevalent conformation in DLPC·LRH-1·TIF2 and just 12.6Å for the dominant apo-LRH-1·SHP conformation (Fig. 8*B*).

Projections of the MD trajectories onto these principal modes (Fig. 8, *C*–*G*) illustrates that DLPC binding promotes conformations with high values of PC2, although apo- and bacterial long-tail lipid-bound states tend to exhibit conformations of lower PC2 magnitude. Co-regulator binding influences the

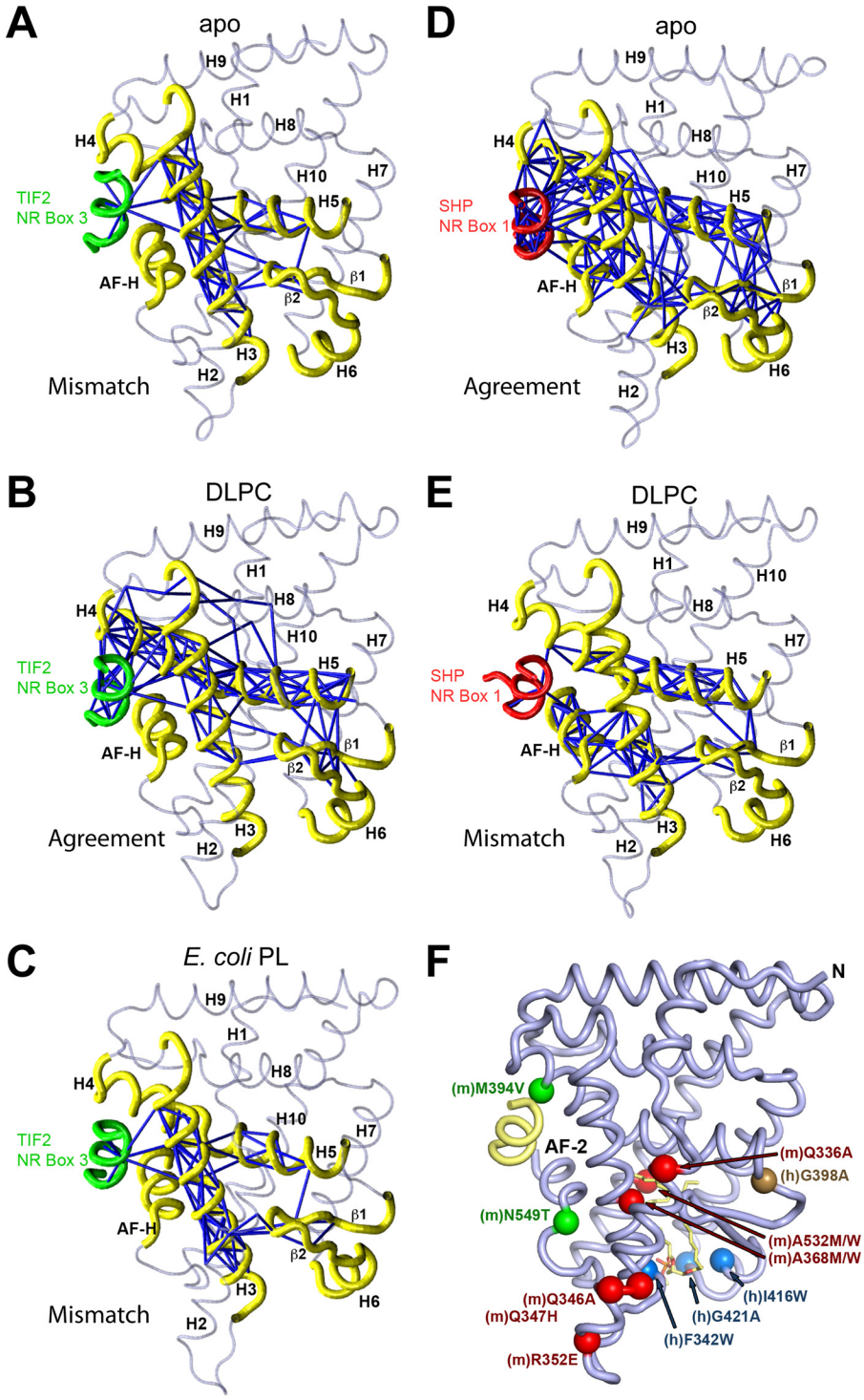

FIGURE 7. **Allosteric paths from binding pocket to co-regulator.** Allosteric communication pathways between the β-sheet-H6 and co-regulator binding regions of the LRH-1 LBD in the apo-LRH-1·TIF2 (*A*), LRH-1·DLPC·TIF2 (*B*), LRH-1·*E. coli* PL·TIF2 (*C*), apo-LRH-1·SHP (*D*), and LRH-1·DLPC·SHP (*E*) complexes. Schematic loop view of LRH-1 showing thick loops (*yellow*, LRH-1; *green*, TIF2; *red*, SHP) for regions of the protein identified along the allosteric path. *F*, LRH-1 mutations that alter PL binding or co-regulator recruitment lie on or adjacent to the allosteric pathway. Known mutations of mouse (*m*) or human (*h*) LRH-1 LBD are shown as C-α spheres on the LRH-1 protein backbone. Mutations shown in *green* enhance the degree of LRH-1 activation in response to co-activator binding; mutations shown in *red* selectively decrease LRH-1 sensitivity to SHP without affecting overall activation; mutations shown in *brown* decrease overall LRH-1 activity without affecting PL binding; mutations shown in *blue* decrease PL binding and overall activity.

dominant conformation's placement along PC1, with all TIF2-bound complexes exhibiting primary centroids near +10 and SHP-bound complexes exhibiting centroids near −10. It is worth noting that the long-tail *E. coli* lipid and apo-TIF2 complexes both share two common clusterings, with the former maintaining nearly equal populations near each center and the latter undergoing a population shift toward the repression promoting region of the subspace. These results show that lipid binding and co-regulator binding both impact motions in the LRH-1 LBD and that combinations of those motions result in

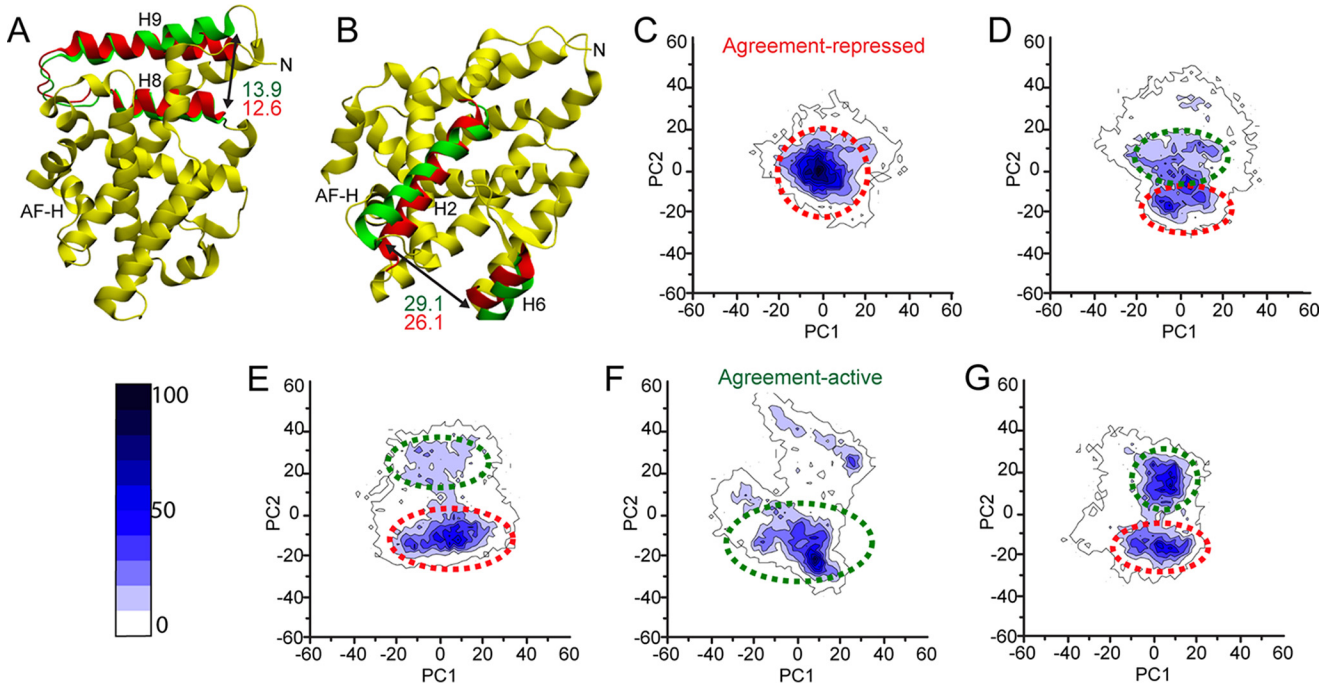

FIGURE 8. **Biologically relevant principal modes identified from the projections of the MD trajectories on PC1 *versus* PC2.** An outward swing of helix 9 contributes to PC1 (*A*), whereas opening motions at the mouth of the lipid binding pocket results in translation along PC2 (*B*). Projections of snapshots were taken from MD onto PC1 and PC2 in apo-LRH-1·SHP (*C*), LRH-1·DLPC·SHP (*D*), apo-LRH-1·TIF2 (*E*), LRH-1·DLPC·TIF2 (*F*), and LRH-1·*E. coli* PL·TIF2 (*G*) complexes. Higher densities indicate more populated regions of the conformational subspace. *Scale bar* indicates how many snapshots (out of 10,000) were collected within a contour. *Green* and *red rings* indicate activating and repressing regions of the subspace, respectively.

TABLE 2
Modes chosen for PC1 and PC2 and the dot products between these modes

PC1	apo SHP : 2	dlpc SHP : 3	apo TIF : 3	dlpc TIF : 3	pl TIF : 3	Average	+/-
apo SHP : 2	1.0000	0.0756	0.0626	0.4221	0.4954	0.4111	0.3834
dlpc SHP : 3	0.0756	1.0000	0.1587	0.4538	0.2609	0.3898	0.3692
apo TIF : 3	0.0626	0.1587	1.0000	0.2138	0.2337	0.3338	0.3783
dlpc TIF : 3	0.4221	0.4538	0.2138	1.0000	0.6050	0.5389	0.2931
pl TIF : 3	0.4954	0.2609	0.2337	0.6050	1.0000	0.5190	0.3112

PC2	apo SHP : 4	dlpc SHP : 1	apo TIF : 1	dlpc TIF : 1	pl TIF : 1	Average	+/-
apo SHP : 4	1.0000	0.3522	0.0943	0.5088	0.0987	0.4108	0.3734
dlpc SHP : 1	0.3522	1.0000	0.1388	0.5782	0.2195	0.4578	0.3457
apo TIF : 1	0.0943	0.1388	1.0000	0.1446	0.0122	0.2780	0.4071
dlpc TIF : 1	0.5088	0.5782	0.1446	1.0000	0.3446	0.5153	0.3184
pl TIF : 1	0.0987	0.2195	0.0122	0.3446	1.0000	0.3350	0.3923

* Modes and dot products were selected for PC1 and PC2 via root mean square inner product. Each system label is formatted as "binding pocket state co-regulator: mode." Averages of dot products and standard deviations for each system with the respect to each other system are included. In each PC, the LRH-1·DLPC·TIF2 system (highlighted in green) was the most central eigenvector, having the highest average inner product with the other systems.

only two distinct and stable conformations, repressing and activating. We also observed that "disagreement" complexes exist in mixed populations between the two states.

The r.m.s.d. alignment of the resultant repressing and activating structures (Fig. 8, *A* and *B*), respectively, reveals that an upward shift in helices 2 and 3 in the activated structure perturbs the AF-H backbone by an r.m.s.d. of 1.2 Å. This alters the binding position of the co-regulator and provides a mechanism by which binding pocket status directly impacts co-regulator choice through PC2. Similarly, overlying the average repressing structure from both the apo-LRH-1-TIF and apo-LRH-1·SHP, the differing binding position of the co-regulator presses outward on helix 4, causing a slight rearrangement in helices 8 and 9, leading to the motion observed in PC1. Interestingly, the large motions identified in PC1 and PC2 encompass the same regions showing the highest conformational movement in previous HDX studies (see supplemental Fig. 3 in Ref. 20). In these prior studies, apo-LRH-1 shows rapid exchange in helices 2, 3,

and 6 (PC1) and helices 8 and 9 (PC2) with complete exchange of these elements occurring in 60 s. These same elements are the most sensitive to ligand status showing the strongest projection in the LRH-1·phospholipid complex.

Modest Disruption of Interhelical Interactions along the Allosteric Pathway Reduces, but Does Not Eliminate, LRH-1 Activity—To verify that the allosteric pathway we identified plays a role in LRH-1 transcriptional activity, we generated mutant forms of LRH-1 designed to perturb the communication network between phospholipid and co-regulator. We took care to avoid residues that make direct contact with the ligand, the AF-2 (co-regulator binding) surface, or the β-sheet-H6 (alternate AF) region because these would all be expected to reduce LRH-1 transactivation. We instead sought to disrupt LRH-1's allostery one shell of residues away from these surfaces. Helix 5 was identified as a central feature of the pathway (Fig. 7, *D* and *B*), as its junction with helix 10 creates the cleft against which helix 12 docks to establish the AF-2 co-regulator binding surface (Fig. 9*A*). Moreover, the acyl tails of long chain PLs dock against these helices. We hypothesized that differences in tail length or unsaturation may exert variable amounts of pressure against these helices, which is then transmitted along the allosteric network to the AF-2 site, affecting co-regulator binding. The junction between helices 5 and 10 displays hydrogen bonding between residues Ser-383 and Glu-514, and electrostatic interactions between residues Glu-384 and Arg-507 (Fig. 9*B*). To disrupt these interactions, we generated mutant forms of LRH-1 (S383A, E384Q/R507H, and S383A/E384Q/R507H) and measured their transcriptional activity in HEK 293T cells via luciferase reporter gene assay.

These mutant forms of LRH-1 all showed a slight decrease in basal activity, which achieved statistical significance specifically upon disruption of the electrostatic interaction between Glu-384 and Arg-507 (Fig. 9*C*). Importantly, none of these mutations fully abrogated LRH-1 activity, indicating that these mutations did not fatally inactivate the receptor.

Discussion

Robust signaling pathways must not only respond to activating ligands but must discriminate against the wrong ones to reduce noise (50). For LRH-1, this challenge is amplified because its ligands include highly abundant intact PLs that include a large fraction of cell membranes. It is possible that LRH-1 displays an intrinsic set of selection criteria for PL isoforms, that PL delivery to the receptor is facilitated by soluble lipid transport proteins, or a combination of the two. Our results show that LRH-1 is able to bind a wide range of PLs *in vitro* but can extract only PCs, PGs, and phosphatidylinositols from a membrane/vesicle without assistance from a molecular chaperone. Inclusion of a nonspecific lipid chaperone, β-cyclodextrin, permits the binding of all glycerophospholipids tested. This is in line with structural studies because the majority of recognition occurs via contacts with the lipid tails and phosphoglycerol backbone. Thus, LRH-1 lipid preference is driven more so by the composition of the PL tails than by the headgroup, which protrudes from the receptor surface. Remarkably, although LRH-1 can readily accommodate a range of medium chain saturated PLs, affinity is high-

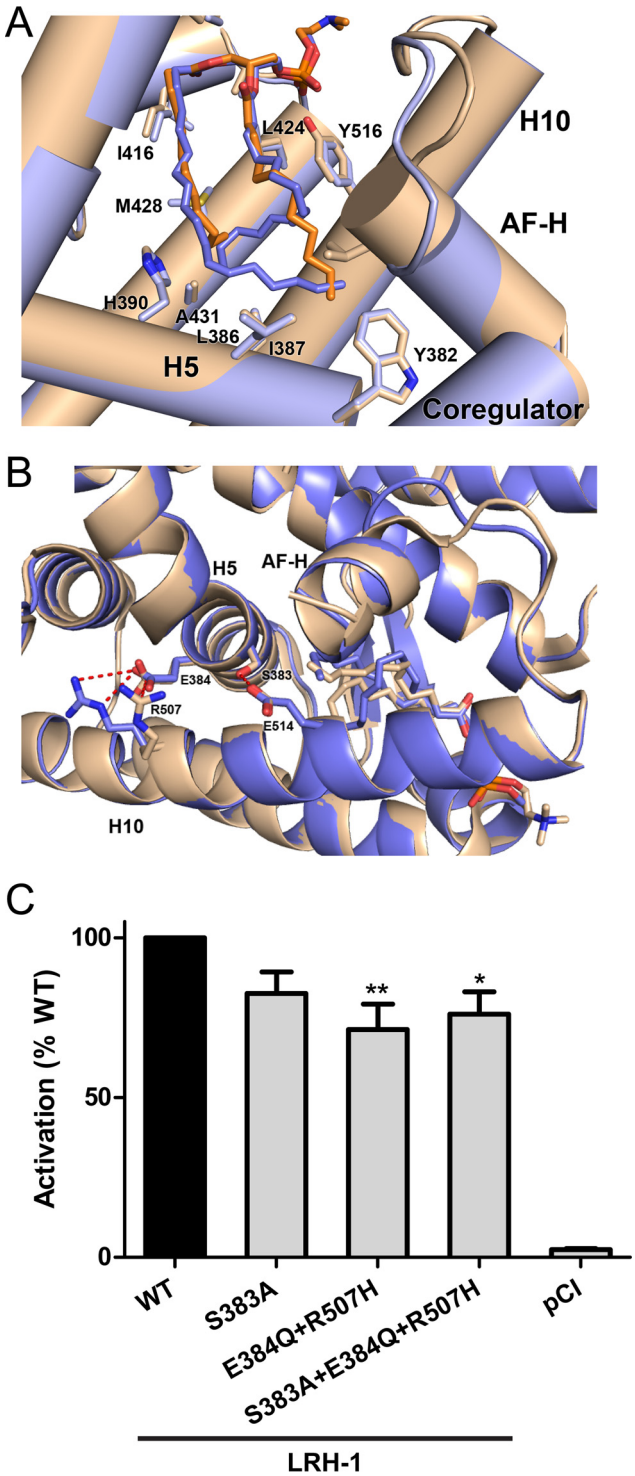

FIGURE 9. **Subtle disruption of residues on or near the allosteric pathway reduces LRH-1 activation.** *A*, close-up view of the PL binding pocket of DLPC- (*beige/orange*) and *E. coli* PL-bound LRH-1 (*blue*). Helices are shown as *cylinders*, and helix 3 has been hidden. Residues within 4.2 Å of the phospholipid are depicted as *sticks*. *B*, junction of helices 5 and 10 displays hydrogen bonding (*red dashes*) between Ser-383 and Glu-514 and electrostatic interactions between Glu-384 and Arg-507. In the active conformation, helix 12 docks against this junction to support the AF-2 co-regulator binding surface, driving gene transactivation and transrepression. *C*, abolition of the electrostatic interaction between helices 5 and 10 via the E384Q/R507H mutation causes a subtle but significant reduction in LRH-1 transcriptional activity. LRH-1 activity was measured via luciferase reporter gene assay in transiently transfected HEK 293T cells. Data are the combined results of five independent experiments. Statistical significance is represented as *, $p < 0.05$; **, $p < 0.01$.

est for the 11- and 12-carbon PCs shown to selectively drive receptor activation in cells (13).

Lipid-mediated Allosteric Control of a Protein-Protein Binding Interface—Intact PLs are unusual ligands, and LRH-1 has evolved to respond to them via a novel allosteric pathway to support appropriate interaction with co-regulators depending on the ligand status. The idea that ligand binding can drive the selective recruitment of different co-regulators has been hypothesized before; previous MD studies have indicated that the SHP/LRH-1 interaction is weakened upon the binding of PS to the apo-receptor, although binding of DAX-1 and PROX1 is strengthened (51), suggesting that an avenue exists for communication between the ligand binding pocket and the AF-2 cleft. Although no studies have demonstrated a role for PS in the regulation of LRH-1's target genes, recent HDX studies that compared LRH-1 bound to *E. coli* PLs and DLPC demonstrated increased flexibility in both the mouth of the ligand binding pocket and the AF-2 region in DLPC-bound LRH-1 (20). Furthermore, stabilizing the mouth of the LBP in apo-hLRH-1 by replacing residues 419–424 with the corresponding mouse LRH-1 sequence enhances binding of the co-activators TIF-2 and PGC1α (52). In the absence of PLs, the receptor accesses a greater amount of conformational space and readily interacts with co-repressors. Medium chain PLs appear to promote productive motions that favor co-activator interaction and disfavor SHP interaction, perhaps by suppressing non-activating (non-productive) motions to drive selective interaction with co-regulators. LRH-1's allosteric network connecting the β-sheet-H6 region may be an evolutionary adaptation that allowed LRH-1 to sense these unusually large ligands and discriminate against fatty acids and cholesterol-derived ligands, which would also fit in the receptor's large hydrophobic pocket.

Ideally, structure-function work should be performed and interpreted in the context of the full-length protein. Obtaining a structure of the intact receptor has been challenging, likely due to the large amount of disorder in the linker region connecting the DNA and ligand binding domains. Thus, we modeled systems for which there was empirical structural and biochemical data. In addition, LRH-1 transactivation has been shown to be affected by post-translational modifications located on the hinge (*i.e.* phosphorylation, acetylation, and SUMOylation) (12). Phosphorylation of the serine residues Ser-238 and Ser-243 in the hinge region of the human LRH-1 by the mitogen-activated protein kinase ERK1/2 enhances its activity (62). LRH-1 also been shown to be acetylated in the basal state and is bound by SHP·sirtuin 1 (SIRT1) transrepressive complex. Surprisingly SIRT1 does not modulate LRH-1 directly, thus what is driving the acetylation and deacetylation of LRH-1 is not established (63). LRH-1 transactivation is also controlled by small ubiquitin-like modifier conjugation to lysine 289 (47). SUMOylation was shown to drive LRH-1 localization in nuclear bodies, whereby small ubiquitin-like modifier-conjugated LRH-1 is preferentially sequestered in these bodies preventing it from binding to DNA (47). Recently, the K. Schoonjans lab showed that SUMOylated LRH-1 interacts with PROX-1, a co-repressor, to control 25% of LRH-1 gene targets in the liver. Mutation of lysine 289 to an arginine specifically ablates PROX-1 interaction, without affecting other canonical co-regulator interactions.

Emerging evidence suggests that NR activation does not occur via the classically described "mouse trap" model, whereby the AF-H swings from an inactive to active state upon agonist binding. Both experimental and modeling studies are inconsistent with radical repositioning of H12 away from the AF-2 in apo-NRs (53–56). Rather, subtle local conformational adaptations are observed in H12 as well as other regions within the ligand binding pocket such as the H11-H12 loop, H3, and H5 (56). These subtle conformational differences between structures may be functionally important, representing a shift between conformational ensembles, but are difficult to identify via inspection of superimposed crystal structures. Previous work with both steroid receptors and fatty acid-sensing NRs have also revealed remarkable flexibility in this region comprising bottom half of the ligand binding pocket, including H3, H6-H7, and H11 (57, 58). In the absence of ligand, NRs are partially unfolded. Recent NMR studies focused on PPARγ show that in the apo-state only half of the expected peaks appear on the intermediate exchange time scale (milliseconds-to-microseconds). NMR supports a model whereby NRs sample a range of conformations in the apo-state. Full-agonists drive this equilibrium toward a more classically active conformation by protecting residues comprising the ligand binding pocket and AF-2 from intermediate exchange, although partial agonists only partially stabilize the regions of the receptor (59). The β-sheet region may also play an important role in mediating PPARγ's response to ligands (53). Although the dynamics in this region are important for mediating ligand action, activation by partial agonists is mediated by the ability of a solvent-inaccessible serine residue in this region to be phosphorylated (53).

Given LRH-1's limited selectivity criteria *in vitro*, it is possible that access to endogenous ligands is controlled both temporally and spatially by phospholipid transfer proteins. For example, phospholipid transfer proteins such as phosphatidylinositol transfer protein α and phosphatidylcholine transfer protein are both capable of transporting intact PLs into the nucleus (60, 61). The effect of tail unsaturation has also not yet been studied, but it is likely that the bends introduced by cis unsaturation would allow the LRH-1 ligand binding pocket to accommodate longer chain acyl tails promoting potent receptor activation. Given the diverse composition of PL tails *in vivo*, these studies are best guided by lipidomics-based identification of endogenous PL ligands. Current limitations in the ability to isolate LRH-1 from mammalian tissue have limited the field's ability to identify endogenous ligands, although these studies are underway.

Author Contributions—P. M. M., B. R. K., J. A. K., I. I., and E. A. O. participated in research design. P. M.M., B. R. K., and J. A. K. conducted the experiments. P. M. M., B. R. K., J. A. K., I. I., and E. A. O. performed data analysis. P. M. M., B. R. K., J. A. K., I. I., and E. A. O. wrote or contributed to the writing of the manuscript.

Acknowledgments—Computational resources were provided in part by National Science Foundation XSEDE Allocation CHE110042 and Allocation m1254 at the National Energy Research Scientific Computing Center supported by the United States Department of Energy Office of Science Contract DE-AC02-05CH11231.

References

1. Musille, P. M., Kohn, J. A., and Ortlund, E. A. (2013) Phospholipid–driven gene regulation. *FEBS Lett.* **587,** 1238–1246
2. Blind, R. D., Sablin, E. P., Kuchenbecker, K. M., Chiu, H. J., Deacon, A. M., Das, D., Fletterick, R. J., and Ingraham, H. A. (2014) The signaling phospholipid PIP3 creates a new interaction surface on the nuclear receptor SF-1. *Proc. Natl. Acad. Sci. U.S.A.* **111,** 15054–15059
3. Liu, S., Brown, J. D., Stanya, K. J., Homan, E., Leidl, M., Inouye, K., Bhargava, P., Gangl, M. R., Dai, L., Hatano, B., Hotamisligil, G. S., Saghatelian, A., Plutzky, J., and Lee, C. H. (2013) A diurnal serum lipid integrates hepatic lipogenesis and peripheral fatty acid use. *Nature* **502,** 550–554
4. Walker, A. K., Jacobs, R. L., Watts, J. L., Rottiers, V., Jiang, K., Finnegan, D. M., Shioda, T., Hansen, M., Yang, F., Niebergall, L. J., Vance, D. E., Tzoneva, M., Hart, A. C., and Näär, A. M. (2011) A conserved SREBP-1/phosphatidylcholine feedback circuit regulates lipogenesis in metazoans. *Cell* **147,** 840–852
5. Fernandez-Marcos, P. J., Auwerx, J., and Schoonjans, K. (2011) Emerging actions of the nuclear receptor LRH-1 in the gut. *Biochim. Biophys. Acta* **1812,** 947–955
6. Moore, D. D., JaeMan, L., and Binging, D. (2010) Targeting nuclear receptors to treat type 2 diabetes. *Endocr. J.* **57,** 75
7. Oosterveer, M. H., and Schoonjans, K. (2014) Hepatic glucose sensing and integrative pathways in the liver. *Cell. Mol. Life Sci.* **71,** 1453–1467
8. Zhang, C., Large, M. J., Duggavathi, R., DeMayo, F. J., Lydon, J. P., Schoonjans, K., Kovanci, E., and Murphy, B. D. (2013) Liver receptor homolog-1 is essential for pregnancy. *Nat. Med.* **19,** 1061–1066
9. Gerrits, H., Paradé, M. C., Koonen-Reemst, A. M., Bakker, N. E., Timmer-Hellings, L., Sollewijn Gelpke, M. D., and Gossen, J. A. (2014) Reversible infertility in a liver receptor homolog-1 (LRH-1)-knockdown mouse model. *Reprod. Fertil. Dev.* **26,** 293–306
10. Kelly, V. R., Xu, B., Kuick, R., Koenig, R. J., and Hammer, G. D. (2010) Dax1 up-regulates Oct4 expression in mouse embryonic stem cells via LRH-1 and SRA. *Mol. Endocrinol.* **24,** 2281–2291
11. Venteclef, N., Jakobsson, T., Steffensen, K. R., and Treuter, E. (2011) Metabolic nuclear receptor signaling and the inflammatory acute phase response. *Trends Endocrinol. Metab.* **22,** 333–343
12. Stein, S., and Schoonjans, K. (2015) Molecular basis for the regulation of the nuclear receptor LRH-1. *Curr. Opin. Cell Biol.* **33,** 26–34
13. Lee, J. M., Lee, Y. K., Mamrosh, J. L., Busby, S. A., Griffin, P. R., Pathak, M. C., Ortlund, E. A., and Moore, D. D. (2011) A nuclear-receptor-dependent phosphatidylcholine pathway with antidiabetic effects. *Nature* **474,** 506–510
14. Bolado-Carrancio, A., Riancho, J. A., Sainz, J., and Rodríguez-Rey, J. C. (2014) Activation of nuclear receptor NR5A2 increases Glut4 expression and glucose metabolism in muscle cells. *Biochem. Biophys. Res. Commun.* **446,** 614–619
15. Mamrosh, J. L., Lee, J. M., Wagner, M., Stambrook, P. J., Whitby, R. J., Sifers, R. N., Wu, S. P., Tsai, M. J., Demayo, F. J., and Moore, D. D. (2014) Nuclear receptor LRH-1/NR5A2 is required and targetable for liver endoplasmic reticulum stress resolution. *eLife* **3,** e01694-e01694
16. Whitby, R. J., Dixon, S., Maloney, P. R., Delerive, P., Goodwin, B. J., Parks, D. J., and Willson, T. M. (2006) Identification of small molecule agonists of the orphan nuclear receptors liver receptor homolog-1 and steroidogenic factor-1. *J. Med. Chem.* **49,** 6652–6655
17. Whitby, R. J., Stec, J., Blind, R. D., Dixon, S., Leesnitzer, L. M., Orband-Miller, L. A., Williams, S. P., Willson, T. M., Xu, R., Zuercher, W. J., Cai, F., and Ingraham, H. A. (2011) Small molecule agonists of the orphan nuclear receptors steroidogenic factor-1 (SF-1, NR5A1) and liver receptor homolog-1 (LRH-1, NR5A2). *J. Med. Chem.* **54,** 2266–2281
18. Corzo, C. A., Mari, Y., Chang, M. R., Khan, T., Kuruvilla, D., Nuhant, P., Kumar, N., West, G. M., Duckett, D. R., Roush, W. R., and Griffin, P. R. (2015) Antiproliferation activity of a small molecule repressor of liver receptor homolog 1. *Mol. Pharmacol.* **87,** 296–304
19. Benod, C., Carlsson, J., Uthayaruban, R., Hwang, P., Irwin, J. J., Doak, A. K., Shoichet, B. K., Sablin, E. P., and Fletterick, R. J. (2013) Structure-based discovery of antagonists of nuclear receptor LRH-1. *J. Biol. Chem.* **288,** 19830–19844
20. Musille, P. M., Pathak, M. C., Lauer, J. L., Hudson, W. H., Griffin, P. R., and Ortlund, E. A. (2012) Antidiabetic phospholipid-nuclear receptor complex reveals the mechanism for phospholipid-driven gene regulation. *Nat. Struct. Mol. Biol.* **19,** 532–537
21. Goodwin, B., Jones, S. A., Price, R. R., Watson, M. A., McKee, D. D., Moore, L. B., Galardi, C., Wilson, J. G., Lewis, M. C., Roth, M. E., Maloney, P. R., Willson, T. M., and Kliewer, S. A. (2000) A regulatory cascade of the nuclear receptors FXR, SHP-1, and LRH-1 represses bile acid biosynthesis. *Mol. Cell* **6,** 517–526
22. Zhi, X., Zhou, X. E., He, Y., Zechner, C., Suino-Powell, K. M., Kliewer, S. A., Melcher, K., Mangelsdorf, D. J., and Xu, H. E. (2014) Structural insights into gene repression by the orphan nuclear receptor SHP. *Proc. Natl. Acad. Sci. U.S.A.* **111,** 839–844
23. Goodwin, B., Watson, M. A., Kim, H., Miao, J., Kemper, J. K., and Kliewer, S. A. (2003) Differential regulation of rat and human CYP7A1 by the nuclear oxysterol receptor liver X receptor-α. *Mol. Endocrinol.* **17,** 386–394
24. Lu, T. T., Makishima, M., Repa, J. J., Schoonjans, K., Kerr, T. A., Auwerx, J., and Mangelsdorf, D. J. (2000) Molecular basis for feedback regulation of bile acid synthesis by nuclear receptors. *Mol. Cell* **6,** 507–515
25. Ortlund, E. A., Lee, Y., Solomon, I. H., Hager, J. M., Safi, R., Choi, Y., Guan, Z., Tripathy, A., Raetz, C. R., McDonnell, D. P., Moore, D. D., and Redinbo, M. R. (2005) Modulation of human nuclear receptor LRH-1 activity by phospholipids and SHP. *Nat. Struct. Mol. Biol.* **12,** 357–363
26. Otwinowski, Z., and Minor, W. (1997) Processing of x-ray diffraction data collected in oscillation mode. *Methods Enzymol.* **276,** 307–326
27. Murshudov, G. N., Skubák, P., Lebedev, A. A., Pannu, N. S., Steiner, R. A., Nicholls, R. A., Winn, M. D., Long, F., and Vagin, A. A. (2011) REFMAC5 for the refinement of macromolecular crystal structures. *Acta Crystallogr. D Biol. Crystallogr.* **67,** 355–367
28. Echols, N., Grosse-Kunstleve, R. W., Afonine, P. V., Bunkóczi, G., Chen, V. B., Headd, J. J., McCoy, A. J., Moriarty, N. W., Read, R. J., Richardson, D. C., Richardson, J. S., Terwilliger, T. C., and Adams, P. D. (2012) Graphical tools for macromolecular crystallography in PHENIX. *J. Appl. Crystallogr.* **45,** 581–586
29. Nicholls, R. A., Fischer, M., McNicholas, S., and Murshudov, G. N. (2014) Conformation-independent structural comparison of macromolecules with ProSMART. *Acta Crystallogr. D Biol. Crystallogr.* **70,** 2487–2499
30. Wang, J., Wang, W., Kollman, P. A., and Case, D. A. (2006) Automatic atom type and bond type perception in molecular mechanical calculations. *J. Mol. Graph. Model.* **25,** 247–260
31. Brooks, B. R., Bruccoleri, R. E., Olafson, B. D., States, D. J., Swaminathan, S., and Karplus, M. (1983) CHARMM: a program for macromolecular energy, minimization, and dynamics calculations. *J. Comput. Chem.* **4,** 187–217
32. Phillips, J. C., Braun, R., Wang, W., Gumbart, J., Tajkhorshid, E., Villa, E., Chipot, C., Skeel, R. D., Kalé, L., and Schulten, K. (2005) Scalable molecular dynamics with NAMD. *J. Comput. Chem.* **26,** 1781–1802
33. Tuckerman, M., Berne, B. J., and Martyna, G. J. (1992) Reversible multiple time scale molecular-dynamics. *J. Chem. Phys.* **97,** 1990–2001
34. Essmann, U., Perera, L., Berkowitz, M. L., Darden, T., Lee, H., and Pedersen, L. G. (1995) A smooth particle mesh Ewald method. *J. Chem. Phys.* **103,** 8577–8593
35. Glykos, N. M. (2006) Software news and updates. Carma: a molecular dynamics analysis program. *J. Comput. Chem.* **27,** 1765–1768
36. Sethi, A., Eargle, J., Black, A. A., and Luthey-Schulten, Z. (2009) Dynamical networks in tRNA:protein complexes. *Proc. Natl. Acad. Sci. U.S.A.* **106,** 6620–6625
37. Humphrey, W., Dalke, A., and Schulten, K. (1996) VMD: visual molecular dynamics. *J. Mol. Graph.* **14,** 33–38

38. Sablin, E. P., Krylova, I. N., Fletterick, R. J., and Ingraham, H. A. (2003) Structural basis for ligand-independent activation of the orphan nuclear receptor LRH-1. *Mol. Cell* **11,** 1575–1585
39. Wang, W., Zhang, C., Marimuthu, A., Krupka, H. I., Tabrizizad, M., Shelloe, R., Mehra, U., Eng, K., Nguyen, H., Settachatgul, C., Powell, B., Milburn, M. V., and West, B. L. (2005) The crystal structures of human steroidogenic factor-1 and liver receptor homolog-1. *Proc. Natl. Acad. Sci. U.S.A.* **102,** 7505–7510
40. Krylova, I. N., Sablin, E. P., Moore, J., Xu, R. X., Waitt, G. M., MacKay, J. A., Juzumiene, D., Bynum, J. M., Madauss, K., Montana, V., Lebedeva, L., Suzawa, M., Williams, J. D., Williams, S. P., Guy, R. K., *et al.* (2005) Structural analyses reveal phosphatidyl inositols as ligands for the NR5 orphan receptors SF-1 and LRH-1. *Cell* **120,** 343–355
41. Blind, R. D., Suzawa, M., and Ingraham, H. A. (2012) Direct modification and activation of a nuclear receptor-PIP2 complex by the inositol lipid kinase IPMK. *Sci. Signal.* **5,** ra44
42. Schaaf, G., Ortlund, E. A., Tyeryar, K. R., Mousley, C. J., Ile, K. E., Garrett, T. A., Ren, J., Woolls, M. J., Raetz, C. R., Redinbo, M. R., and Bankaitis, V. A. (2008) Functional anatomy of phospholipid binding and regulation of phosphoinositide homeostasis by proteins of the sec14 superfamily. *Mol. Cell* **29,** 191–206
43. Kanno, K., Wu, M. K., Scapa, E. F., Roderick, S. L., and Cohen, D. E. (2007) Structure and function of phosphatidylcholine transfer protein (PC-TP)/StarD2. *Biochim. Biophys. Acta* **1771,** 654–662
44. Schouten, A., Agianian, B., Westerman, J., Kroon, J., Wirtz, K. W., and Gros, P. (2002) Structure of apo-phosphatidylinositol transfer protein alpha provides insight into membrane association. *EMBO J.* **21,** 2117–2121
45. Nagy, L., and Schwabe, J. W. (2004) Mechanism of the nuclear receptor molecular switch. *Trends Biochem. Sci.* **29,** 317–324
46. Li, Y., Lambert, M. H., and Xu, H. E. (2003) Activation of nuclear receptors: a perspective from structural genomics. *Structure* **11,** 741–746
47. Chalkiadaki, A., and Talianidis, I. (2005) SUMO-dependent compartmentalization in promyelocytic leukemia protein nuclear bodies prevents the access of LRH-1 to chromatin. *Mol. Cell. Biol.* **25,** 5095–5105
48. Levy, R. M., Srinivasan, A. R., Olson, W. K., and McCammon, J. A. (1984) Quasi-harmonic method for studying very low frequency modes in proteins. *Biopolymers* **23,** 1099–1112
49. Skjaerven, L., Martinez, A., and Reuter, N. (2011) Principal component and normal mode analysis of proteins; a quantitative comparison using the GroEL subunit. *Proteins* **79,** 232–243
50. Atkins, W. M. (2015) Biological messiness *vs.* biological genius: mechanistic aspects and roles of protein promiscuity. *J. Steroid Biochem. Mol. Biol.* **151,** 3–11
51. Burendahl, S., Treuter, E., and Nilsson, L. (2008) Molecular dynamics simulations of human LRH-1: the impact of ligand binding in a constitutively active nuclear receptor. *Biochemistry* **47,** 5205–5215
52. Musille, P. M., Pathak, M., Lauer, J. L., Griffin, P. R., and Ortlund, E. A. (2013) Divergent sequence tunes ligand sensitivity in phospholipid-regulated hormone receptors. *J. Biol. Chem.* **288,** 20702–20712
53. Hughes, T. S., Chalmers, M. J., Novick, S., Kuruvilla, D. S., Chang, M. R., Kamenecka, T. M., Rance, M., Johnson, B. A., Burris, T. P., Griffin, P. R., and Kojetin, D. J. (2012) Ligand and receptor dynamics contribute to the mechanism of graded PPARγ agonism. *Structure* **20,** 139–150
54. Martínez, L., Polikarpov, I., and Skaf, M. S. (2008) Only subtle protein conformational adaptations are required for ligand binding to thyroid hormone receptors: simulations using a novel multipoint steered molecular dynamics approach. *J. Phys. Chem. B* **112,** 10741–10751
55. Batista, M. R., and Martínez, L. (2013) Dynamics of nuclear receptor Helix-12 switch of transcription activation by modeling time-resolved fluorescence anisotropy decays. *Biophys. J.* **105,** 1670–1680
56. Mackinnon, J. A., Gallastegui, N., Osguthorpe, D. J., Hagler, A. T., and Estébanez-Perpiñá, E. (2014) Allosteric mechanisms of nuclear receptors: insights from computational simulations. *Mol. Cell. Endocrinol.* **393,** 75–82
57. Bledsoe, R. K., Montana, V. G., Stanley, T. B., Delves, C. J., Apolito, C. J., McKee, D. D., Consler, T. G., Parks, D. J., Stewart, E. L., Willson, T. M., Lambert, M. H., Moore, J. T., Pearce, K. H., and Xu, H. E. (2002) Crystal structure of the glucocorticoid receptor ligand binding domain reveals a novel mode of receptor dimerization and co-activator recognition. *Cell* **110,** 93–105
58. Gee, A. C., and Katzenellenbogen, J. A. (2001) Probing conformational changes in the estrogen receptor: evidence for a partially unfolded intermediate facilitating ligand binding and release. *Mol. Endocrinol.* **15,** 421–428
59. Kojetin, D. J., and Burris, T. P. (2013) Small molecule modulation of nuclear receptor conformational dynamics: implications for function and drug discovery. *Mol. Pharmacol.* **83,** 1–8
60. Nile, A. H., Bankaitis, V. A., and Grabon, A. (2010) Mammalian diseases of phosphatidylinositol transfer proteins and their homologs. *Clin. Lipidol.* **5,** 867–897
61. Kang, H. W., Kanno, K., Scapa, E. F., and Cohen, D. E. (2010) Regulatory role for phosphatidylcholine transfer protein/StarD2 in the metabolic response to peroxisome proliferator activated receptor alpha (PPARα). *Biochim. Biophys. Acta* **1801,** 496–502
62. Lee, Y. K., Choi, Y. H., Chua, S., Park, Y. J., and Moore, D. D. (2006) Phosphorylation of the hinge domain of the nuclear hormone receptor LRH-1 stimulates transactivation. *J. Biol. Chem.* **281,** 7850–7855
63. Chanda, D., Xie, Y. B., and Choi, H. S. (2010) Transcriptional co-repressor SHP recruits SIRT1 histone deacetylase to inhibit LRH-1 transactivation. *Nucleic Acids Res.* **38,** 4607–4619